Vertical Gradients in Fluidized Sand Columns

Joy Foley, Civil and Environmental Engineering, Colorado School of Mines, Golden, Colorado, United States

Introduction

The utilization of earthen water-retaining structures has been a part of civilization for thousands of years. Earthen dams and levees (EDLs) are an important component in twenty-first-century infrastructure, providing water storage, flood protection, waste containment, and renewable energy. Internal erosion is the most common failure mechanism of EDLs (Bonelli, 2013). Figure 1 shows an example of the effects of internal erosion in an embankment. Unlike external erosion, which can be physically observed, internal erosion occurs either within or below an embankment and can initiate and progress undetected. Even when evidence of internal erosion is observed, it is challenging to know the extent of the erosion and the structure's risk of failure. The ability to predict, detect, and characterize internal erosion is crucial for designing safe new structures and assessing and the health of existing structures.

Figure 1: Internal Erosion Failure, Australia (Fell & Fry, 2005)

Backwards piping erosion (piping) is one of the four recognized initiation mechanisms of internal erosion. This mechanism involves the loosening and transportation of soil particles from the embankment or foundation of a structure due to hydraulic pressures caused by seepage. The engineering communities' understanding of piping has evolved considerably in the past century, beginning as purely empirical guidelines in the early 1900's (Robbins, 2014) and expanding to the current state of the practice, wherein laboratory and numerical models seek to couple empirical observations with the laws of physics.

Figure 2 shows a simplified sketch of an EDL experiencing piping. As indicated by the figure, the erosion channel consists of a horizontal (1) and a vertical (2) flow path. Piping within the horizontal flow path has

been studied extensively by researchers including Dr. Vera Van Beek (van Beek, 2015), Dr. Hans Sellmeijer (Sellmeijer & Koenders, 1991), and Robin Fell (Fell & Fry, 2013). Conversely, piping within the vertical flow path has not been studied extensively (Koelewijn, 2009). For a given structure, the gradients and corresponding head losses within the horizontal and vertical branches are dependent upon each other (i.e. higher head loss/gradients within the vertical branch correspond to lower head loss/gradients within the horizontal branch, and vice versa). Therefore, the head losses and piping behaviors within the vertical flow path must be understood in order to understand the erosional process as a whole.
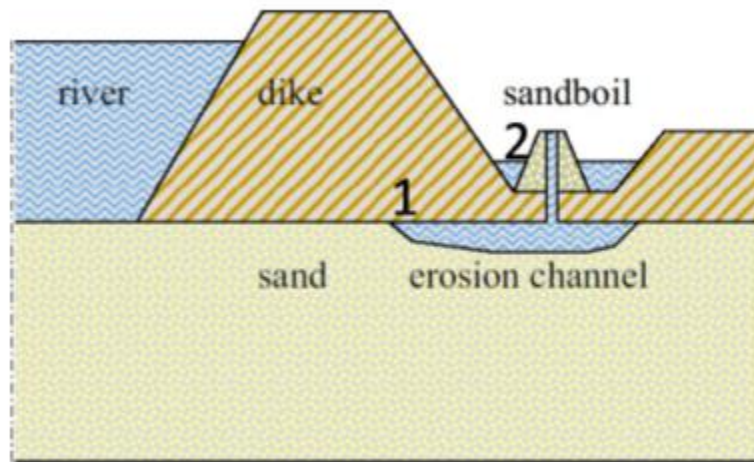

Figure 2: Piping Channel with Horizontal (1) and Vertical (2) Flow Paths (Bezuijen, 2015)

Research Objectives

The purpose of this study was to investigate gradients within vertical columns of soil experiencing piping. The research questions specifically addressed in this study were:

1. What is the numerical relationship between specific flow rate and hydraulic gradient within a column of fluidized sand?
2. How is this relationship influenced by the diameter of the fluidized column of sand and by the grain size and grain size distribution of the fluidized sand?

Literature Review/Background

Overview of Internal Erosion

Internal erosion is the removal of soil particles from the embankment or foundation of an EDL due to seepage forces (Fell & Fry, 2007). The four recognized initiation mechanisms of internal erosion are

suffusion/suffosion, concentrated leak erosion, contact erosion, and backwards piping erosion, which are defined as follows (Fell & Fry, 2005), (Van Beek, Bezuijen, & Sellmeijer, 2013), (Brown & Bridle, 2008):

Suffusion/Suffosion: the washout of relatively fine soil particles from a body of soil. Occurs in internally unstable soils in which the fine particles are freely "floating" within a coarse soil matrix.

Concentrated Leak Erosion: the scouring of soil particles due to increased specific velocity of seepage flow concentrated through a crack or hydraulic fracture caused by settlement, desiccation, or freezing and thawing in an EDL. Occurs in soils capable of sustaining an open crack or in the interconnecting voids within a permeable soil.

Contact Erosion: the washout of fine soil particles into a coarser soil matrix. Occurs due to seepage flow parallel to a horizontal contact between a fine soil overlying a coarse soil with an ineffective filter.

Backward Piping Erosion (Piping): The loosening and migration of soil particles from the foundation or embankment of an EDL through an unfiltered exit face on the downstream side of an EDL. Occurs due to high exit and overall gradients and unprotected seepage faces downstream of the structure.

These initiation mechanisms can occur simultaneously or in series within a structure. This study focuses primarily on backward piping erosion (piping). Piping initiates on the downstream side of an EDL and progressively works its way towards the upstream side, hence the name "backwards" piping erosion. This erosion process eventually forms a system of one or more eroded preferential pathways referred to as "pipes" within the foundation and/or embankment of the EDL. Although piping can occur within a variety of soil types, it typically occurs in uniform, cohesionless sands (Van Beek, Bezuijen, & Sellmeijer, 2013).

In order for piping to occur, the following four conditions must exist (Fell & Fry, 2005), (Mattsson, Hellstrom, & Lundstrom, 2008), (Van Beek, Bezuijen, & Sellmeijer, 2013):

- A source of water (e.g. a reservoir) contributing a hydraulic gradient across an EDL and a consequential seepage flow beneath an EDL
- Erodible material within the foundation or embankment of an EDL that can be transported by seepage flow (e.g. a uniform sand)
- An unprotected/unfiltered exit through which the eroded material can be transported
- Cohesive, low-permeability material overlying the pipe that can form a stable "roof", preventing the collapse of the overlying material and the destruction of the pipe (e.g. an overlying clay layer)

These four conditions are commonly found in river levees in the Netherlands, along the Mississippi River in the U.S., and along the Yangtze and Nenjiang Rivers in China, and evidence of piping has been observed

at all of these locations (Van Beek, Bezuijen, & Sellmeijer, 2013). When all four of these conditions are met, piping can occur and is broken down into four phases:

1) Initiation
2) Continuation
3) Progression
4) Breach/failure.

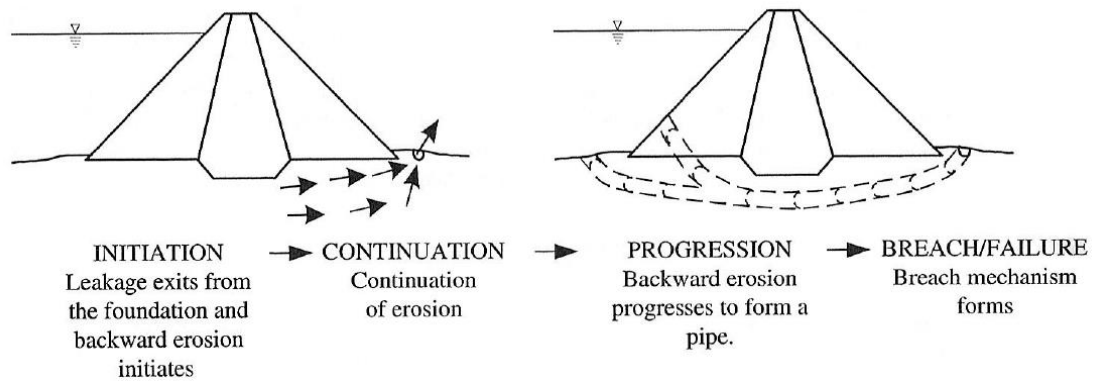These phases are illustrated in Figure 3 (Fell & Fry, 2007) and are described in further detail below.

INITIATION → CONTINUATION → PROGRESSION → BREACH/FAILURE
Leakage exits from the foundation and backward erosion initiates / Continuation of erosion / Backward erosion progresses to form a pipe. / Breach mechanism forms

Figure 3: Four Phases of Piping Leading to Failure (Fell & Fry, 2007)

Initiation: Soil particles on the downstream side of the EDL begin to be detached from the soil matrix. This can be the detachment of individual particles or the fluidization of a column of soil, which is referred to in the literature as heave, fluidization, or liquefaction.

Continuation: Soil particles continue to be transported by seepage. This stage requires a lack of filtration or protection against soil transport at the exit point of the flow. The transported soil particles are deposited on the ground surface downstream of the embankment, forming sand volcanos or "sand boils", shown in Figure . The appearance and growth of sand boils on the downstream side of an EDL are indications of the initiation and continuation of piping.

Progression: The detachment and transportation of soil particles moves progressively upstream, creating a system of continuous flow channels (pipes). This stage requires a cohesive and stable overlying roof for the developing pipes to remain open. Otherwise, the overlying material will likely collapse, destroying the pipes.

Breach/Failure: The pipes extend to the reservoir upstream of the EDL and continue to grow, resulting in unregulated flow beneath the EDL, slope instability, unravelling of the face of the EDL, and/or overtopping due to settlement or the development of sinkholes.

EDLs are often designed with an impervious blanketing layer downstream of the embankment. When there is a covering layer (e.g. a clay cap) on the downstream side of an ELD and blowout or hydraulic fracturing occurs, a vertical seepage path is created with a length equal to the thickness of the cover. If high hydraulic pressures continue, this seepage path becomes filled with fluidized sand, which offers some resistance to piping. However, there is no unified method for evaluating the influence of a sand-filled vertical pipe on the head loss within a structure. The currently utilized methods to account for resistance within vertical flow paths are highly empirical.

Initial Empirical Observations

The first quantitative studies of piping within water retaining structures were conducted by Colonel John Clibborn and John Stuart Beresford, who investigated the failure of the Khanki Weir on the Chenab River in India in 1895 (Robbins, 2014). Clibborn and Beresford conducted flow tests through sands representative of the foundations of numerous levees in India. Clibborn's findings broadened the understanding of hydraulic gradient lines across EDLs and called attention to a linear relationship between hydraulic gradients and piping susceptibility within EDLs (Skempton, 1984), (Van Beek V. M., 2015). Beresford's research proved the effectiveness of using filters to prevent piping. After Beresford used his results to accurately predict the failure of the Narora Weir on the Ganges River, designers began taking hydraulic gradients into account (Lane, 1935).

Shortly after Clibborn and Beresford's observations, William George Bligh, a British engineer with experience with dams and weirs in India, Egypt, Canada, and the USA, sought to define a numerical relationship between hydraulic gradients and piping susceptibility. Using Darcy's Law in conjunction with data and observations from failed dams and weirs, Bligh developed a design factor known as the percolation coefficient, c, which is defined as the critical minimum ratio between the seepage path length, L, and differential head, H, required to initiate piping, as shown in Equation 1 and Figure 4 (Bligh, 1910):

$$\frac{kA}{Q} = \frac{k}{v} = \frac{L}{H} = c \tag{1}$$

where k is the hydraulic conductivity of the soil, A is the cross-sectional area of flow, Q is volumetric seepage flowrate, and v is the linear seepage velocity.
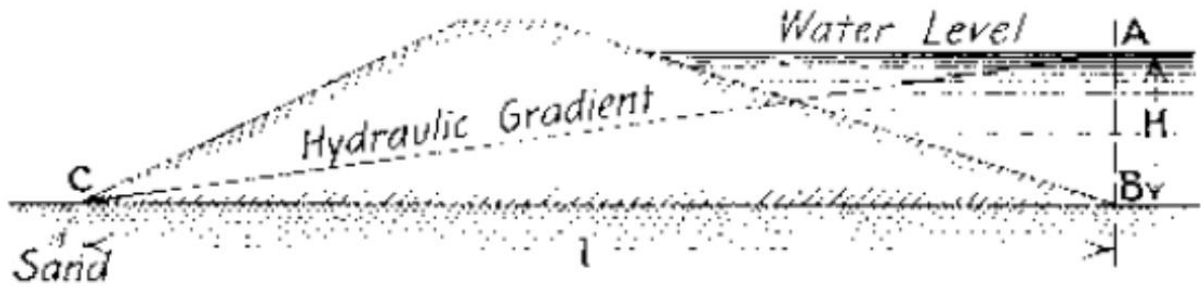
Figure 4: Schematic of Bligh's c-Value Components (Bligh, 1910)

According to Bligh, structures with L/H values less than a pre-determined soil-specific percolation coefficient are susceptible to piping (Bligh, 1915), (Koenig, 1911). Bligh recommended using percolation coefficients he determined experimentally for different types of soil, which are presented in Table 1. When developing Equation 1, Bligh did not account for vertical flow paths and assumed that L was equal to the horizontal length of the structure. These c values are analogous to the inverse of what would later be defined as the critical gradient against piping for a structure.

Table 1: Bligh's Recommended Percolation Coefficients (Bligh, 1910)

Class	Soil Type	c-value
A	Fine silt and sand as in the Nile River	18
B	Fine micaceous sand as in the Colorado and Himalayan Rivers	15
C	Ordinary coarse sand	12
D	Gravel and sand	9
E	Boulders, gravel, and sand	4 to 6

Similar findings were published by W. M. Griffith in 1913, who also considered the three-dimensional nature of seepage flow and described how the formation of an eroded pipe results in a lower-pressure flow path, causing seepage to concentrate towards this path on the downstream side of an EDL, leading to higher local velocities (i.e. higher hydraulic gradients) and making a structure susceptible to internal erosion at relatively low differential heads (Griffith, 1913). Based on these observations, Griffith developed his own suggested L/H design values, shown in Table 2, with the disclaimer that higher values of L/H were recommended for shingles and boulders in order to account for leakage loss, and lower values of L/H would be appropriate for structures that incorporated vertical seepage flow (Griffith, 1913). Bligh and Griffith both assumed that the development and progression of piping would occur along the contact between the structure and foundation material, which because known as the "line-of-creep" theory (Lane, 1935).

Table 2: Griffith's Recommended Percolation Coefficients (Griffith, 1913)

Material	Limiting Safe Value of L/H
Fine micaceous sand	14.5 – 16
Fine quartz sand	12.5 – 14
Coarse quartz sand	10 – 12
Shingle	8
Boulders	4

The first researcher to differentiate numerically between horizontal and vertical flow was E. W. Lane, who, in 1935, published a study of the stability of over 200 water retaining structures founded on permeable soil in order to improve Bligh's method. Using the geometry, geology, and loading conditions experienced by the dams, some of which had failed and some of which had not, Lane concluded that horizontal and gently-sloping flow paths (less than 45° with the horizontal) offered roughly one third the resistance to piping when compared to vertical and steeply-sloping flow paths (greater than 45° with the horizontal) (Lane, 1935). Lane also investigated the line-of-creep theory and speculated that it was not always valid; for some conditions, the path of least resistance for percolation would be directly through the foundation material, which he referred to as the "short-path" theory. From these observations, Lane developed a table of safe weighted-creep ratios, shown in Table 3, which took into account the weighted influences of horizontal and vertical flow and could be modified to account for short-path flow (as opposed to the line-of-creep flow path). These values are analogous to Bligh's percolation coefficients and are meant to be applied to EDL design using Equation 1, where L is the sum of the total vertical flow path length, L_{vert}, and one third of the total horizontal flow length, L_{Horiz}, and is calculated using Equation 2 (Terzaghi & Peck, 1948).

Table 3: Recommended percolation coefficients (Lane, 1935)

Soil Type	Safe weighted-Creep-Ratio, cw
Very fine sand or silt	8.5
Fine sand	7.0
Medium sand	6.0
Coarse sand	5.0
Fine gravel	4.0
Medium gravel	3.5
Coarse gravel, including cobbles	3.0
Boulders with some cobbles and gravel	2.5
Soft clay	3.0
Medium clay	2.0
Hard clay	1.8
Very hard clay, or hardpan	1.6

$$L = \frac{1}{3}\sum L_{Horiz} + \sum L_{Vert} \qquad (2)$$

Historical Laboratory Testing and Numerical Modeling

The design rules presented by Bligh and Lane were widely accepted and used in the construction of EDLs (Robbins, 2014). However, Karl Terzaghi and Ralph B. Peck (1948) pointed out that both methods were entirely empirical and were based on worst-case scenarios associated with historical EDL failures (i.e. maximum c-values and minimum critical heads known to initiate piping). Terzaghi and Peck argued that the recommended c-values were too conservative, resulting in some overdesigned EDLs, and empirical, resulting in some EDLs constructed on unfavorable soil conditions with factors of safety near unity. (Terzaghi & Peck, 1948).

Terzaghi and Peck derived the effective stress-critical gradient approach in order to make the understanding of internal erosion less empirical and more physically-based. This approach uses the principles of effective stress and force equilibrium to determine what vertical flow conditions will initiate internal erosion in an EDL. This concept can be illustrated in Figure 5, where water is flowing upwards from a constant head of h_1 to a constant head of h_2 through a homogeneous soil with a saturated unit weight of γ_{sat}. The effective stress, σ', at an arbitrarily selected point A can be calculated as

$$\sigma' = h_3(\gamma_{sat} - \gamma_w) - (h_1 - h_2)\gamma_w = h_3\gamma' - \Delta h\gamma_w \qquad (3)$$

where γ_w is the unit weight of water, γ' is the buoyant unit weight of the soil, and Δh is the differential head across the soil sample. As the value of h_1 increases, the effective stress at point A decreases. For some value of $\Delta h = h1 - h3$, the effective stress equals zero, and the following condition holds:

$$\frac{\gamma'}{\gamma_w} = \frac{h_3 - h_2}{h_3} = \frac{G_s(1-n)\gamma_w + n\gamma_w - \gamma_w}{\gamma_w} = (G_s - 1)(1 - n) = \frac{G_s - 1}{1 + e} = i_c \qquad (4)$$

where γ' is the buoyant unit weight, G_s is the specific gravity, n is the porosity, and i_c is the critical gradient of the soil (i.e. the gradient required to reduce effective stress at point A to zero). The value of i_c in this equation is commonly approximated as 1.0 given typical values of Gs and e, although erosion has been known to initiate at overall gradients of less than 1.0 (Rice & Swainston-Fleshman, 2013). These lower initiation gradients could be attributed to concentrated flow paths, which would cause localized hydraulic gradients to exceed overall gradients. When the critical gradient is reached, the soil will be in what is known as a quick-condition, heave, liquefaction, or fluidization, wherein the soil acts as a liquid-solid material. It should be noted that Equation 4 is valid for any point within the vertical soil column.

This approach was based on the assumption that, at a given critical gradient, an entire sand-filled column subjected to upwards vertical flow will experience liquefaction. It should be noted that this approach considers a local hydraulic gradient corresponding to upwards vertical flow and not the global hydraulic gradient acting across the entire EDL, which consists of horizontal and vertical flow. Equation 4 was only meant to describe critical gradients for piping initiation and was not meant as a tool for calculating subsequent hydraulic gradients after piping has begun.
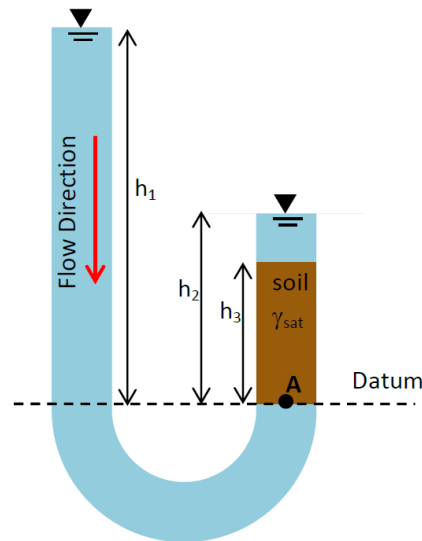

Figure 5: Upward seepage through a soil column

In 1937, Arthur Casagrande presented the concept of flownets as the graphical solution to the continuity equation of two-dimensional seepage flow (Casagrande, 1937). Flownets, referred to by Casagrande as Forchheimer's graphical solution, were originally conceived by Phillip Forchheimer (1914). However, Casagrande's publication was the first time the concept had been explained in detail in English (Robbins, 2014). Terzaghi and Peck used flownets to compute expected vertical gradients and the effective stress–critical gradient approach to compute the critical local gradient at the toes of existing structures, in order to estimate the structure's susceptibility to piping initiation.

Although the effective stress–critical gradient approach was useful in determining the risk of liquefaction of a packed column of soil, it failed to address the post-liquefaction behavior of the fluidized soil. To address this unknown, vertical flow tests were performed in 1981 by J. B. Sellmeijer to observe the resistance to piping offered by the fluidized sand within a vertical pipe (Sellmeijer, 1981) (Yap, 1981). The purpose of these flow tests was not to evaluate the accuracy of Equation 4, but to observe the behavior of hydraulic gradients within soil post-fluidization. An illustration of the apparatus used in these tests is shown in Figure 6. Water was flowed upwards through a sand column, and the sand was brought to fluidization. The

downstream head was held at a constant value, and the differential hydraulic head of the system was increased by raising the elevation of the upstream reservoir, resulting in an increase in flow rate. As the flow rate was increased through the sand, the hydraulic gradients across the sample were measured via standpipes spaced vertically along the sand column. Tests were run within plastic tubes with smooth inner walls, plaster-coated inner walls, and sand-coated inner walls. A total of 35 one-dimensional vertical flow tests were run. The results of these tests are shown in Figure, where flow rate is plotted on the x-axis and hydraulic gradient on the y-axis. It was assumed by the author that the Figure 6 only includes hydraulic gradients measured within the sand post-liquefaction. The three graphs on the right-hand side of Figure 6 show the results of all 35 liquefaction tests. The results are segregated by the inner wall conditions (i.e. smooth, plaster-coated, and sand-coated), and are labeled as such.

From all three plots on the right-hand side of Figure 6, it should first be noted that, in general, the soil experienced a maximum hydraulic gradient of roughly 1.0 before liquefying, validating the efficacy of Equation 4. It should also be noted that after liquefaction, the gradient decreases as flow rate increases. This decrease continues until termination at or before a gradient of roughly 0.3. It is unclear whether gradients below 0.3 were never reached due to the nature of the tests, or if the tests were simply terminated at this point, and lower gradients could have been reached had the tests been continued.

From these results Sellmeijer developed the following linear relationship between specific discharge (Q) and the log of the hydraulic gradient (φ/d) within a column of fluidized sand:

$$\frac{Q}{Ak_0} = \ln\left(\alpha \frac{d}{\varphi}\right)$$

(5)

Where A is the cross-sectional area of the pipe, k_0 and α are scaling parameters for the specific discharge and hydraulic gradient, respectively, and are dependent on the type of sand being fluidized, and φ and d are the local differential hydraulic head and flow path length, respectively, within a section of the fluidized sand. This equation is reminiscent of Darcy's Law for flow through packed particulate beds:

$$Q = kiA$$

(6)

However, as opposed to Darcy's Law, which calculates increases in gradients as the flow rate increases, Equation 5 states that, for fluidized soils, as the flow rate increases, the gradients decrease exponentially, meaning that for greater flow rates, fluidized soils offer less resistance to internal erosion. Based on the test results, Sellmeijer also concluded that the type of coating on the inside walls of the tube did not greatly influence the gradients within the fluidized sands. It should be noted that Equation 5 implies a uniform gradient across the entire fluidized soil column.
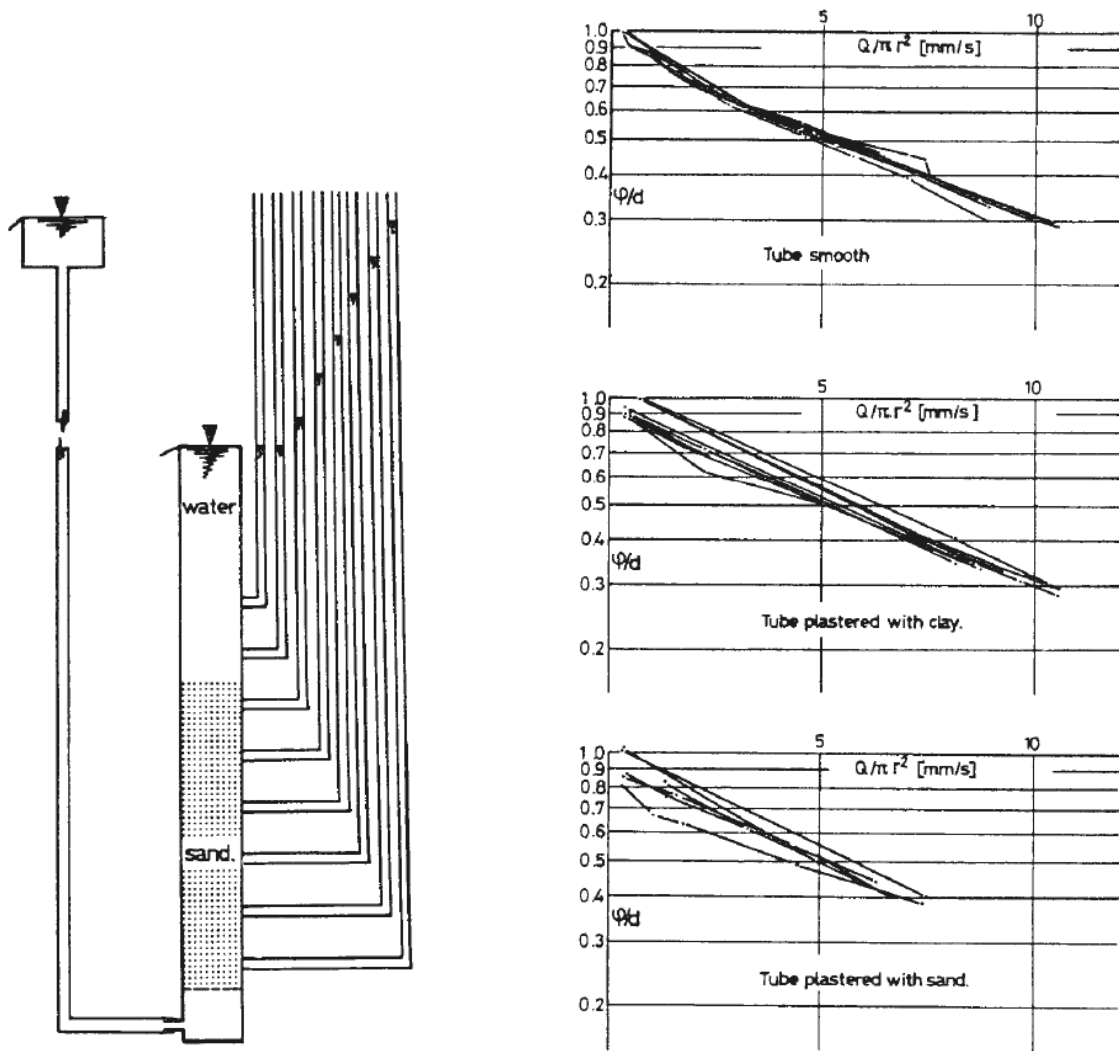
Figure 6: Sellmeijer's Fluidization Test setup and relationship between specific discharge (Q) and hydraulic gradient (φ/d) (Sellmeijer, 1981).

The results of these tests have led researchers to believe that the minimum gradient reached by a fluidized sand column will be 0.3. This belief has influenced levee design in the Netherlands, however, it is currently being questioned (Bezuijen, 2015). Further research is required to come to a more definite conclusion on the topic.

Laboratory Testing at The Colorado School of Mines

Twelve fluidization tests were conducted in a laboratory setting at the Colorado School of Mines. The purpose of Tests 1 through 4 was to observe the influence of the diameter of the fluidized sand column on piping behavior. The purpose of Tests 5 through 12 was to observe the influence of grain size and grain size distribution on piping behavior. These tests are summarized in Table 4.

Test Number	Sand Type Used	Permeameter Diameter (cm)
1	Poorly-Graded	5.25
2	Poorly-Graded	5.25
3	Poorly-Graded	4.09
4	Poorly-Graded	4.09
5	Coarse-Grained	5.25
6	Coarse-Grained	5.25
7	Medium-Grained	5.25
8	Medium-Grained	5.25
9	Fine-Grained	5.25
10	Fine-Grained	5.25
11	Well-Graded	5.25
12	Well-Graded	5.25

Testing Equipment

Two rigid walled permeameters with inner diameters of 5.25 cm and 4.09 cm were designed specifically for this investigation. Both permeameters were designed to subject a column of sand to upwards water flow and were outfitted with five vertically spaced total water pressure transducers. Hydraulic flow was controlled by varying the elevation of an upstream reservoir while maintaining the downstream outflow at a fixed elevation. A schematic of the test setup is shown in Figure . The individual components of the setup are described in more detail in the following sections.
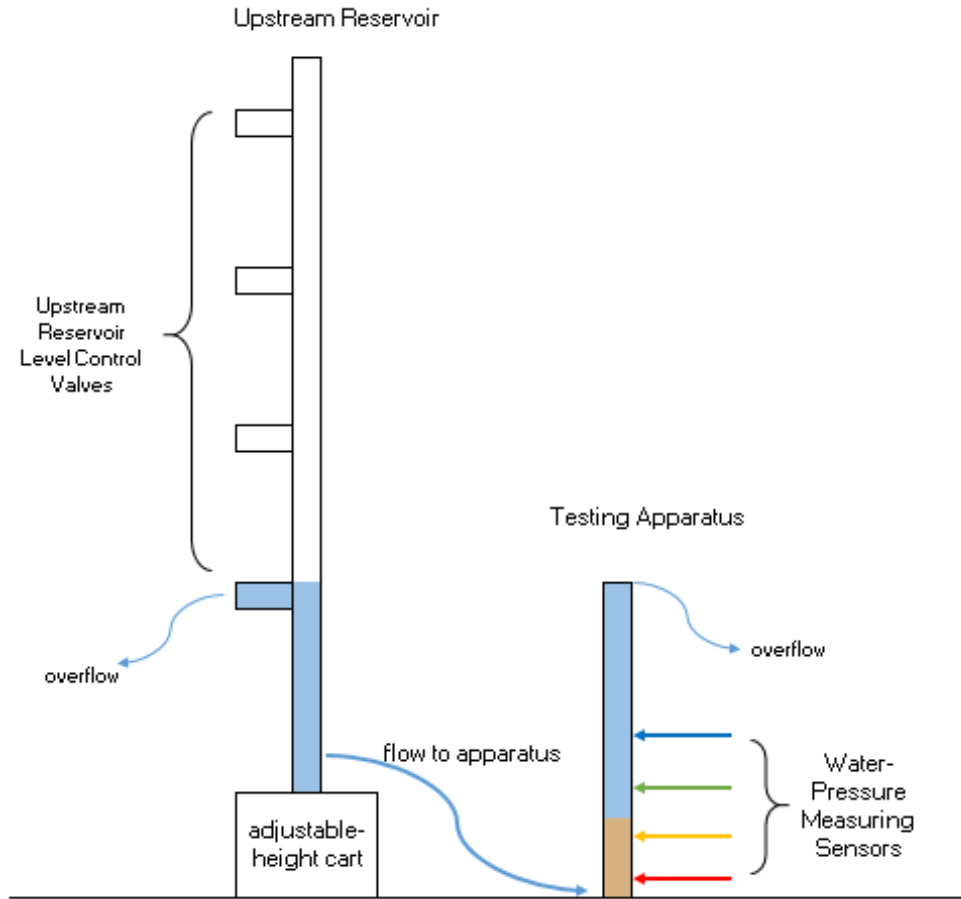
Figure 7: Fluidizaiton Test Setup

Permeameters

The permeameters were designed after Sellmeijer's tests, shown in Figure 6 (Sellmeijer, 1981) and were designated Permeameter A and Permeameter B. The dimensions for each are shown in Table 5, and Figures 8 and 9 show an image of each.

Table 5: Permeameter Dimensions

	Permeameter		Units
	B	C	
Diameter	5.25	4.09	cm
Radius	2.63	2.04	cm
Cross-Sectional Area	21.65	13.13	cm^2

The walls of the permeameters were constructed out of 4-foot long clear PVC pipes. The permeameter bases were constructed out of PVC and brass pipe fittings. Each base included a rigid wire mesh screen,

which retained the sand specimens at a known elevation while allowing water to flow freely upwards through the sand. Each permeameter was fitted with a primary valve to control inflow into the permeameter and a secondary valve to allow for rapid draining of water after each test. Five ports were drilled into the side of each permeameter, which were connected to the total pressure transducers via flexible tubing, visible on Figures 8 and 9. These four transducer ports were spaced vertically at 8.67 cm increments near the base of the permeameter (where they would potentially be in contact with the sand during fluidization tests). The fifth was placed slightly below the outflow port (where it would likely only be in contact with water) to ensure that the measured readings were sensical. The outflow port for each permeameter was drilled into the side at a known elevation.

Figure 8: Permeameter A

Figure 9: Permeameter B

Upstream Reservoir

In order to generate hydraulic flow through the sand within the permeameters, an apparatus had to be constructed that would generate a differential hydraulic head between the upstream and downstream ends of the permeameters. To facilitate this, a reservoir was constructed that allowed the user to set the upstream hydraulic head at a known elevation (and therefore water pressure), while the downstream hydraulic head was held at a constant elevation, as shown on Figure 7. A photograph of this reservoir is shown on Figure 10. The upstream reservoir consisted of a roughly 10-ft-tall PVC pipe with four overflow ports vertically spaced at 62-cm intervals. Each overflow port was fitted with a valve, which were used to control the elevation of water within the reservoir. The reservoir was placed on a variable-height mechanical table that could be manually raised and lowered. Total elevation of the upstream reservoir was equal to the sum of the elevation of the lowest open overflow port from the surface of the table, which was a known value, and the elevation of the table itself, which was measured using a measuring tape shown in Figure 11. Given this setup and the fixed outflow elevation of the permeameters, the minimum and maximum possible differential hydraulic heads that could be applied to a test specimen were 0 and 273.3 cm [0.00 to 3.89 psi], respectively.

Figure 10: Upstream Reservoir

Figure 11: Mechanical Table of Upstream Reservoir

Instrumentation and Measurements

Hydraulic pressures were measured using US161-C00004-100PG Total Pressure Transducers manufactured by Measurement Specialties Inc. with a pressure range of 0 to 100 psi, which was well within the expected pressures for this research project. The transducers were connected to a National Instruments Corporation (NI) Data Acquisition System (DAQ), which was powered by a desktop computer. The DAQ transferred all recorded data using the commercially available software *LabVIEW*, which organized raw voltages measured by the transducers and output them into a text file. The raw data were imported into the commercially available software *MATLAB*, in which they were processed. Data processing is discussed in further detail in the following sections.

Material Tested

Five gradations of silica sand were selected for testing:

1. Poorly-graded
2. Well-graded
3. Coarse-grained (material retained on #20 sieve)
4. Medium-grained (material retained on #40 sieve)
5. Fine-grained (material retained on #60 sieve)

Sands retained on the #20 sieve were selected as the coarsest material, because initial tests run on coarser material experienced limited to no fluidization, likely because larger diameter sands had a larger buoyant unit weight. Sands retained on the #60 sieve were selected as the finest materials, because this was the finest gradation that could be retained by the wire mesh at the base of the permeameters. Grain size distributions of the sands tested are shown on Figure 12. Grain Size distributions for the poorly- and well-graded sands are presented in Tables 6 and 7. The specific gravity was estimated to be 2.6 for all sands.

The initial tests, tests 1, 2, 3, and 4, were run with a poorly-graded silica sand in permeameters A and B. All subsequent tests used the well-graded, coarse-, medium-, and fine-grained sand in permeameter A.
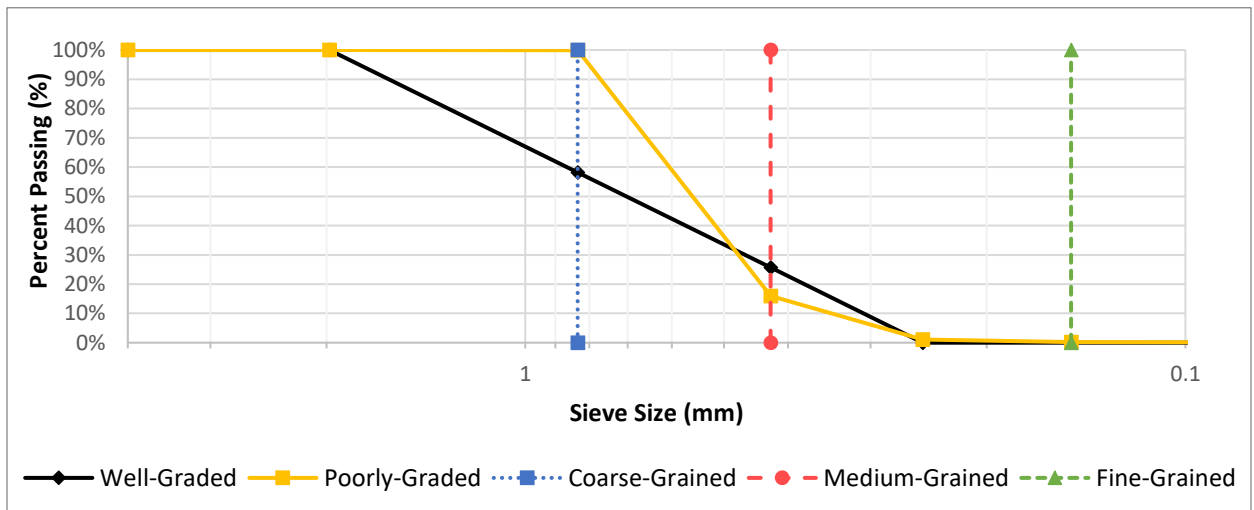
Figure 12: Grain Size Distributions for all five soils tested

Table 6: Poorly-graded Sand Grain Size Distribution

Sieve #	Size (mm)	Mass Retained (g)	% passing
10	1.981	0	100.0%
20	0.833	0.6	99.94%
40	0.425	840.2	15.98%
60	0.250	988.7	1.13%
100	0.149	997.6	0.24%
200	0.075	998.8	0.12%
PAN	0.01	1000	0.00%

Table 7: Well-Graded Sand Grain Size Distribution

Sieve #	Size (mm)	Mass Retained (g)	% passing
10	1.981	0.00	100.0%
20	0.833	334.83	58.15%
40	0.425	594.92	25.64%
60	0.250	800.00	0.00%
PAN	0.010	800	0.00%

Testing Procedure

The testing procedure for all fluidization tests was as follows.

1. 800 grams of oven-dried sand were measured and set aside
2. The appropriate permeameter was attached to a tank of de-aired water and was filled roughly ¾ full
3. The valves between the de-aired water tank and permeameter were closed, and the permeameter was then gently shaken and tapped to release entrapped air.
4. The test sand was pluviated through the water in roughly eight 100 g lifts. Each lift was allowed to settle before the next was placed in order to avoid particle segregation.
5. The sand was kept in the permeameter overnight to allow saturation
6. The following day, the pore pressure transducers were attached to their respective ports using flexible tubing. Care was taken to avoid allowing air bubbles into the instruments, as this could result in data discrepancies.
7. The valves between the de-aired water tank and the permeameter were opened slightly to completely fill the permeameter without disturbing the sand sample.

8. The valves were closed, and the permeameter was disconnected from the de-aired water tank and connected to the upstream reservoir.

9. The pore water pressure transducers were powered and data began being recorded. At least thirty minutes of static pressure data were collected, which were later used to calibrate the measured water pressures.

10. The upstream reservoir cart was set at its lowest elevation, the lowest overflow port of the upstream reservoir was opened, and the reservoir was filled with tap water.

11. While continuing to collect water pressure readings, the valves between the upstream reservoir and the permeameter were opened, and the cart was slightly raised to apply a differential hydraulic head. This was measured using the tape measure affixed to the cart. The initial differential head was, in general, of the order of five to ten centimeters.

12. The differential head was given fifteen minutes to come to equilibrium.

13. After fifteen minutes, the sand height and flow rate were measured.

14. After the differential head had been applied for roughly twenty minutes, the cart was raised again, and Steps 11 through 13 were repeated.

15. When the cart reached its maximum height, the overflow port was closed, the cart was reset to its lowest position, and steps 11 through 14 were repeated for the next highest overflow port. This process was repeated until the cart was at its maximum height and the reservoir was using its highest overflow port. After this final differential hydraulic head had been applied for at least twenty minutes, the test was concluded.

16. The valves between the permeameter and the upstream reservoir were closed and both apparatus were drained.

17. The water pressure transducers were unpowered and disconnected from the permeameter.

18. The sand was removed from the permeameter, and the permeameter was flushed to remove any residual sand

19. The tested sand was placed in an oven and dried overnight.

Data Collection

Data were collected for hydraulic gradients, sand height, and flow rate for each differential hydraulic head applied to the specimen. After a change in differential head was applied to the specimen, the system was allowed to reach equilibrium, which typically took about 15 minutes, before measurements were considered reasonable.

Hydraulic gradients were measured between transducer ports 1, 2, 3, and 4, where 1 is the lowermost port and 4 is the uppermost port in contact with the sand specimen. Gradients are designated as PX-Y, where X

was the lowermost transducer port and Y was the uppermost (e.g. P1-2 refers to the gradient between pore water pressure transducer ports 1 and 2, while P3-4 refers to the gradient between ports 3 and 4). The configuration allowed for six potential gradients: P1-2, P1-3, P1-4, P2-3, P2-4, and P3-4. The sand height was measured using a measuring tape taped to the side of the permeameter, which is visible on Figure 8. Flow rate was measured by collecting and weighing water from the downstream outflow port of the permeameters over a set period of time. Water was collected over a period of 60 seconds for relatively lower flow rates and 30 seconds for relatively higher flow rates. Three flow rate measurements were collected for each differential hydraulic head, and the average of the three was defined as the flow rate. In this process, the water was assumed to have a density of 1 gram per cubic centimeter.

Data Analysis

Pore Water Pressure Transducer Calibration

The pore pressure transducers were scaled and offset to convert their raw voltage readings to total hydraulic heads. The relationship between the measured voltages and applied hydraulic heads is shown in Equation 7 as:

$$V - V_0 = \frac{h_p}{CF} \tag{1}$$

where V is the average voltage reading for a given upstream elevation (volts), V_0 is the offset (volts), h_P is the applied pressure head (cm), and CF is the calculated calibration factor (volts/cm).

To calculate initial offset values, the transducers were placed on a countertop and data were recorded for roughly one hour. The differences between the averaged voltage readings and zero were taken as an initial estimate for the offset values. To calculate calibration factors for the instrumentation, a transducer was connected to the base of the upstream reservoir via flexible tubing. The reservoir was filled to a known elevation, and the connected transducer collected pore pressure data for roughly 30 minutes. The upstream elevation was then raised, and the process was repeated for ten total reservoir elevations. This entire process was repeated for all five transducers. Recorded voltages were averaged for each upstream reservoir elevation, and the resulting data were offset using the initial offset estimates.

Two options were considered for calculating the calibration factors. The first was called the Averaged Ratio method, in which the ratio between offset voltage and expected pore pressure was calculated for each pressure head interval, the calculated ratios were averaged, and the averaged value was used as the calibration factor. The second was called the Line of Best Fit method, in which *Microsoft Excel* was used to generate a line of best fit with an intercept forced through zero for the offset voltage versus expected pressure head values. The slope of this line was used as the calibration factor. In the Averaged Ratio method,

the calibration factor calculation weights each data point equally, which can be advantageous, because higher or lower voltages are not favored in the calculation. However, this method is more sensitive to outliers. The Line of Best Fit method is less sensitive to outliers but gives greater weight to values farther from the origin, because the line of best fit is forced through the origin. In general, both methods underestimated pressure head for low voltages and overestimated pressure head for high voltages. However, for all five transducers, the line of best fit method deviated from higher voltages less than the averaged ratio method. Because this research is more concerned with the behavior of liquified sand at higher flow rates, and therefore higher pressure heads, the Line of Best Fit method was selected to calculate calibration factors for each pore pressure transducer.

To account for instrument drift between tests, a unique secondary offset was assigned to each transducer for each fluidization test. Offsets were calculated by fully saturating the specimen within the permeameter with the pore pressure transducers saturated and connected, shutting off the inflow valve to allow for static flow conditions, attaching the transducers to the DAQ, and allowing the transducers to measure roughly 30 to 60 minutes of static pore pressures. The recorded static readings were scaled, and the difference between the measured pressure head and the expected pressure head for each transducer was used as the offset for that particular test. This method of offsetting was not implemented until Test 5, and offsets for preceding tests were estimated using engineering judgment based on pressure data collected before and after fluidization tests were performed.

Signal Processing

In order to remove electrical noise from the readings collected by the transducers, the raw data were filtered using a low-pass Butterworth filter in *MATLAB*. Figure 13 compares the Butterworth filter with the raw data from a fluidization test in frequency domain. The filtered data were then smoothed in order to increase readability. Figure 14 Compares unfiltered and unsmoothed, filtered and unsmoothed, and filtered and smoothed raw data. From the figure, it can be seen that the filtered and smoothing process significantly improves the readability of the data.
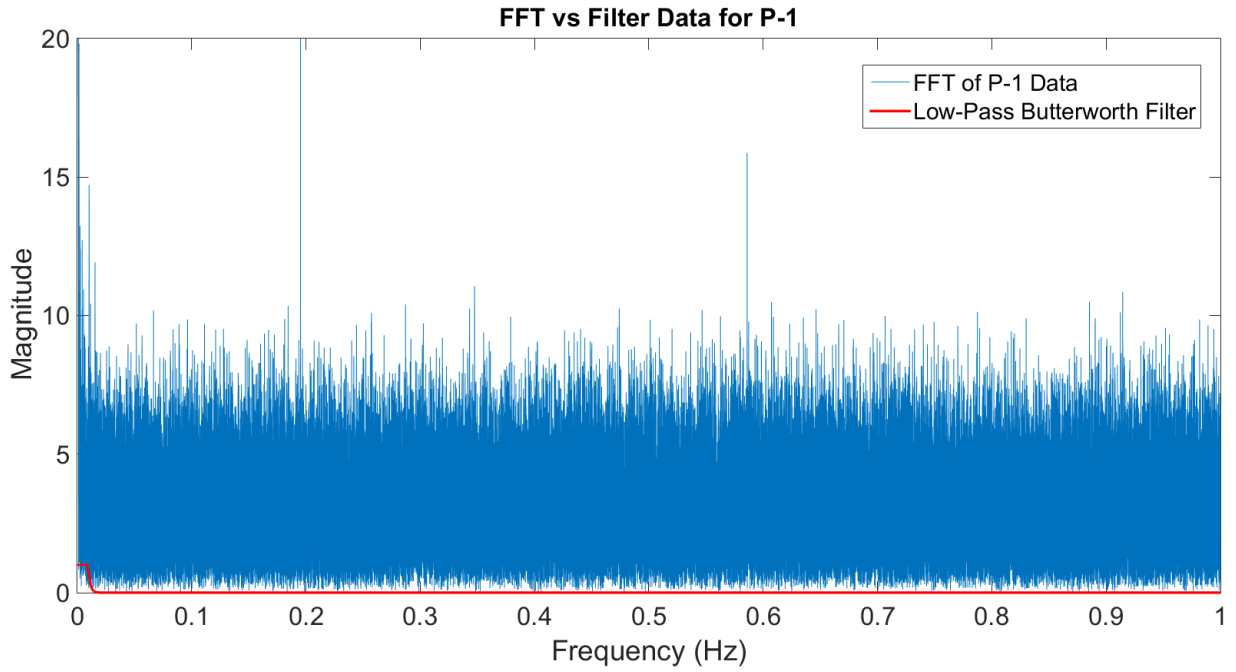
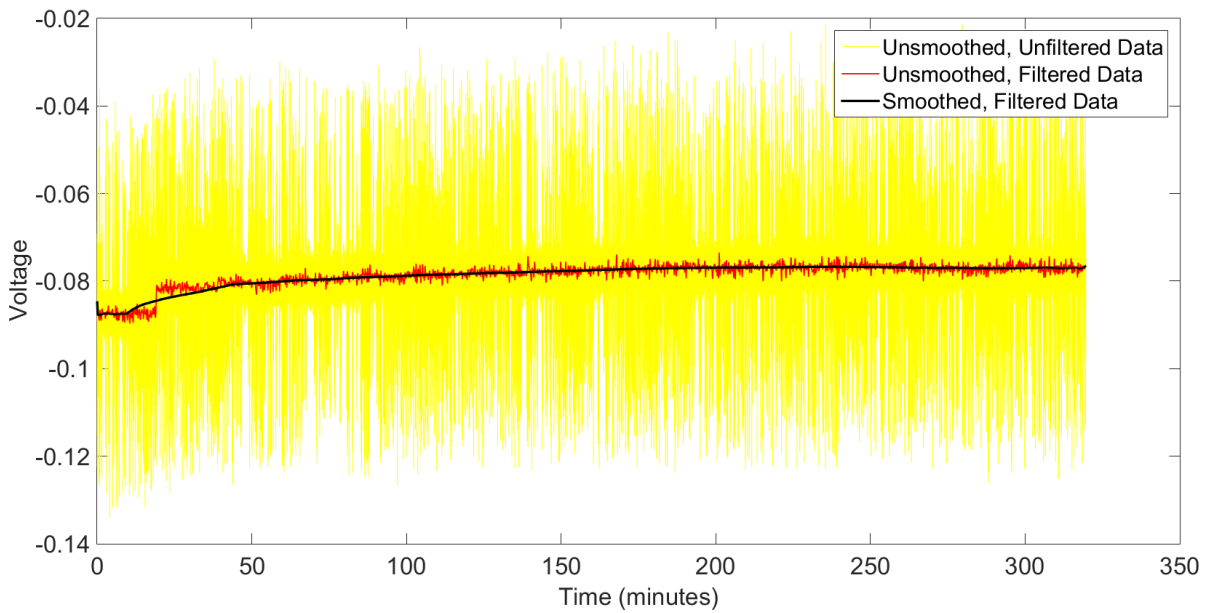*Figure 13: Butterworth Filter Plotted Against FFT of Transducer Data*

Figure 14: Influence of Filtering and Smoothing Raw Data
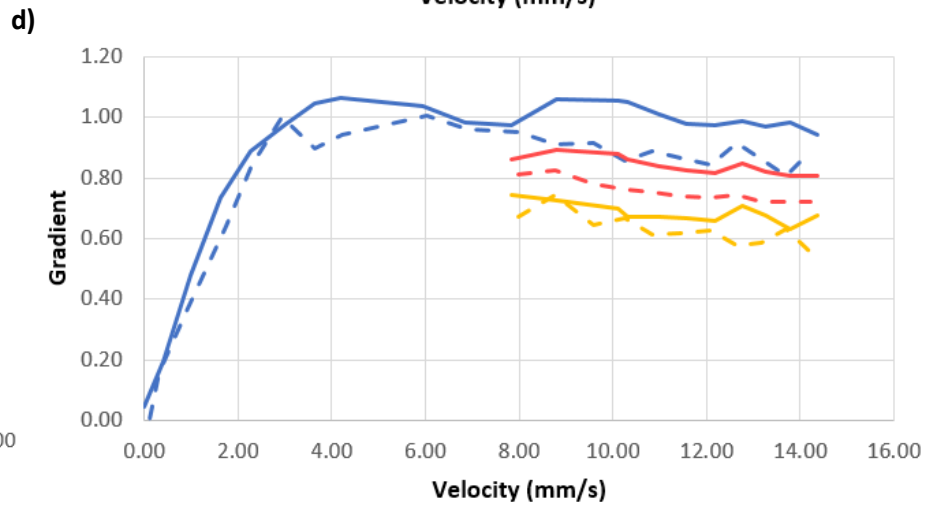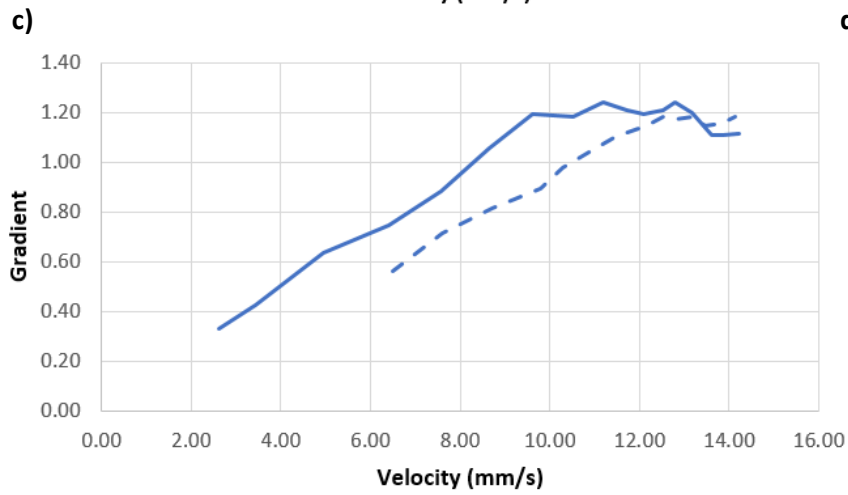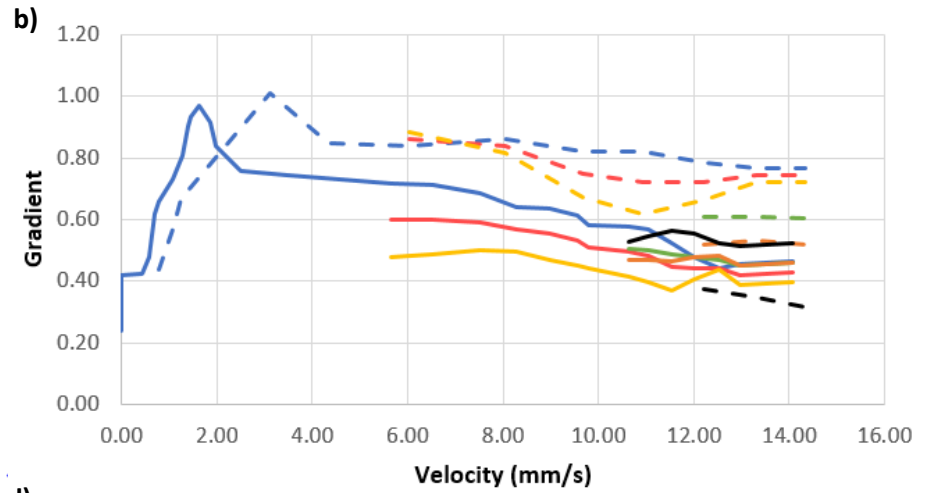
Test Results and Discussion

The 12 test configurations tested are shown in Table 4. This section presents a discussion of the test results. The tests are divided into two stages: (1) pre- and (2) post-fluidization. During Stage 1, hydraulic gradients increased as differential hydraulic heads and flow velocities increased. At some gradient, active sand boils were observed on the top surface of the sand columns. Small increases in column height were also observed during this stage, indicating heave. Stage 1 ended when the maximum gradient was reached. During Stage 2, the sand was considered fluidized. Hydraulic gradients began, in general, to decrease as differential hydraulic heads and flow velocities increased, and the column height continued to increase. As the upstream reservoir was raised, the gradients continued to decrease until the reservoir was at its maximum elevation, marking the end of the test. All test data are presented in Appendix A.

Gradient vs Flow Rate

As previously mentioned, hydraulic gradients were measured between transducer ports 1, 2, 3, and 4. These gradients are plotted against hydraulic flow rate on Figure 15. As indicated in Table 4, two tests were run for each sand type and permeameter diameter combination. Solid lines and dashed lines on Figure 15 are used to differentiate between the two tests for each combination.

During the initial stages of each test, sand was only in contact with the ports of 1 and 2 (ports 3 and 4 were located above the initial elevation of the sand), making P1-2 the only meaningful gradient, shown in Blue in Figure 15. As fluidization caused heave and expansion of the sand column, the sand came into contact with transducers placed higher on the permeameter, allowing for additional gradients to be captured. It should be noted that sand did not expand to higher transducers for every test. For example, the coarse-grained sand (tests 5 and 6) never expanded to the third transducer (3), while the medium-grained (tests 7 and 8) and well-graded sands (tests 11 and 12) expanded to transducer 3, but not transducer 4.

Local gradients during a given test exhibited similar slopes and trends but were not equivalent in value. In general, P1-2 was the highest of all six gradients, while P3-4 was the lowest, with the remaining gradients scattered in between. This suggests that the density of the fluidized sand columns is non-uniform, with higher densities and correspondingly higher resistance to flow, near the base of the column. This seems to contradict the assumptions of Sellmeijer (Sellmeijer, 1981), who claimed that gradients within a fluidized column would be uniform. Additionally, the gradients recorded for a given flow rate were considerably higher than the results in Sellmeijer's 1981 investigation. However, it should be noted that the minimum gradients reached at the end of each test do not represent the minimum possible gradients in the sand column and were limited by the maximum elevation of the upstream reservoir.

Figure 15: Hydraulic Gradients verses Flow Velocities for Tests (a) 1 and 2; (b) 3 and 4; (c) 5 and 6; and (d) 7 and 8

e)

f)
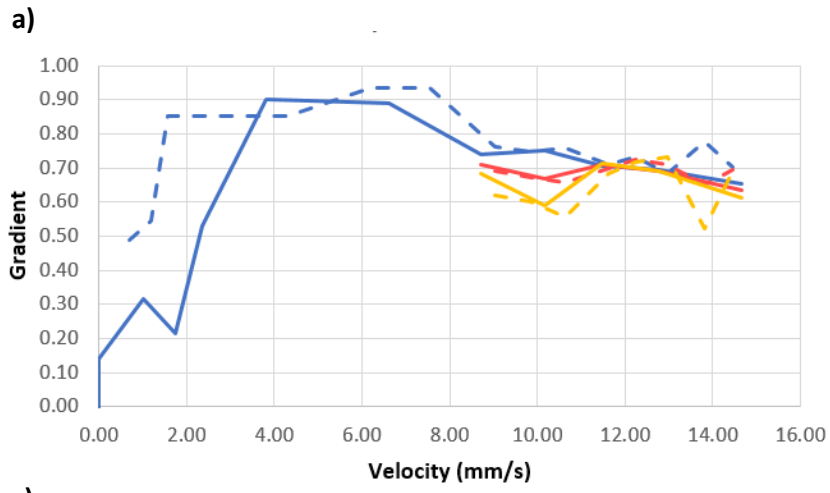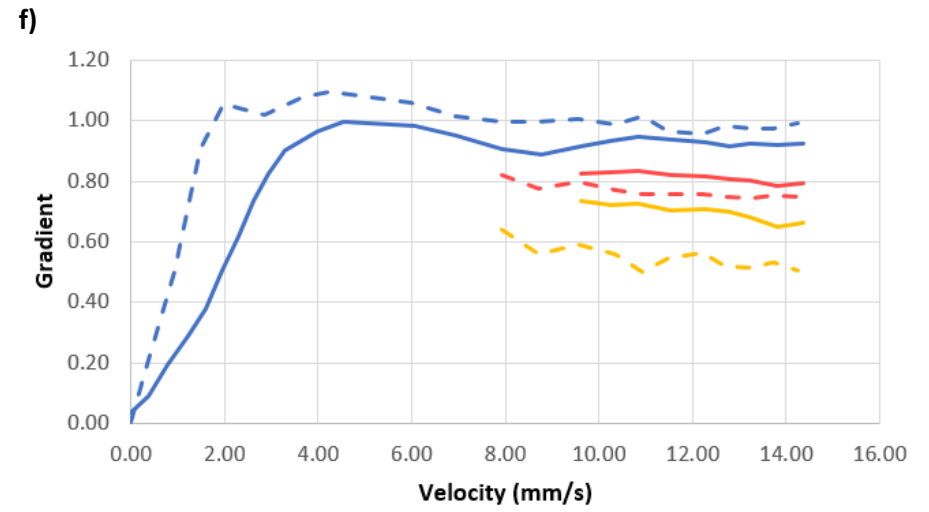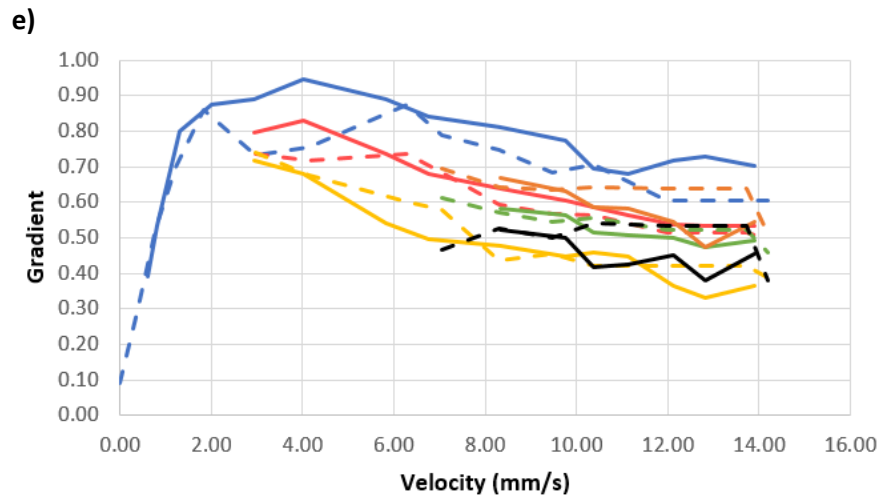
Legend: P1-2 · P1-3 · P1-4 · P2-3 · P2-4 · P3-4 · TEST 1 · — — TEST 2

Figure 15: Hydraluic Gradients verses Flow Velocities for Tests (e) 9 and 10; (f) 11 and 12

Figure 16 and Figure 17 compare the gradients between specific transducer ports. Figure 16 shows data for tests 1, 2, 3, and 4, which plots tests run in the 5.25 cm diameter permeameter in orange and tests run in the 4.09 cm diameter permeameter in yellow. Figure 17 shows data for tests 5, 6, 7, 8, 9, 10, 11, and 12, which plots tests run using the coarse-grained sand in blue, medium-grained sand in pink, fine-grained sand in green, and well-graded sand in black. It should be emphasized that the color designations used in these figures are not related to those used in Figure 15, but the solid and dashed lines still represent the two tests run for each sand and permeameter combination. Because only Tests 3, 4, 9, and 10 observed the fluidized sand reaching port 4, these plots were not considered useful and are not shown here but are available upon request.

Fluidization gradients for the tests run with the poorly-graded sand in Permeameters A and B were between 0.80 and 1.00, which is in accordance with Terzaghi's effective stress theory. All four tests had similar slopes, indicating that gradients decreased at comparable rates as flow rates increased. Figure 16 shows that, although one of the tests conducted in Permeameter B recorded lower gradients than the tests run in Permeameter B, the gradients recorded in the second test run in Permeameter B closely resembled the gradients of both tests run in Permeameter A. From these four tests, it cannot be concluded that diameter contributes a measurable difference in piping behavior.

When comparing the influence of grain size on piping behavior, the coarse-grained sand fluidized at the highest gradient and had the highest minimum gradient after fluidization. The fine-grained sand fluidized at the lowest gradient and had the lowest minimum gradient after fluidization. The medium-grained and well-graded sands had similar behavior, with fluidization and final minimum gradients between those of the course- and fine-grained sands. Before fluidization occurred, the coarse-grained sand had the lowest overall slope in terms of flow rate vs. hydraulic gradient, indicating it had the highest initial hydraulic conductivity. After fluidization, all eight tests had similar slopes, indicating similar dissipation of resistance to piping.
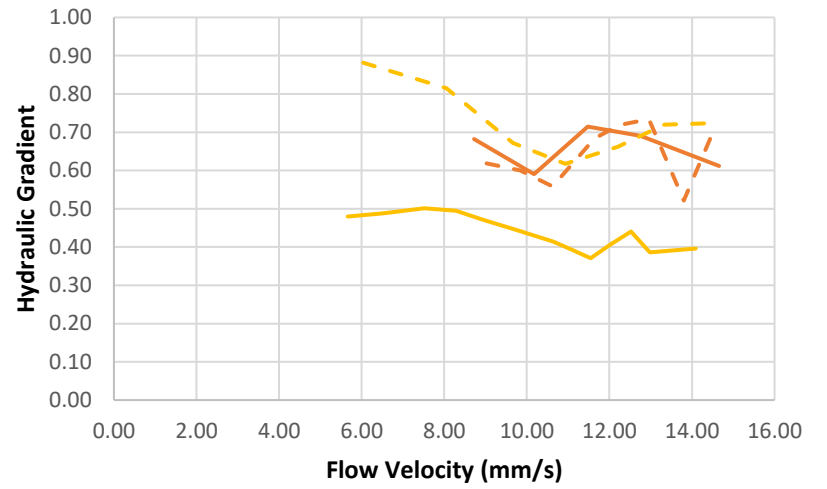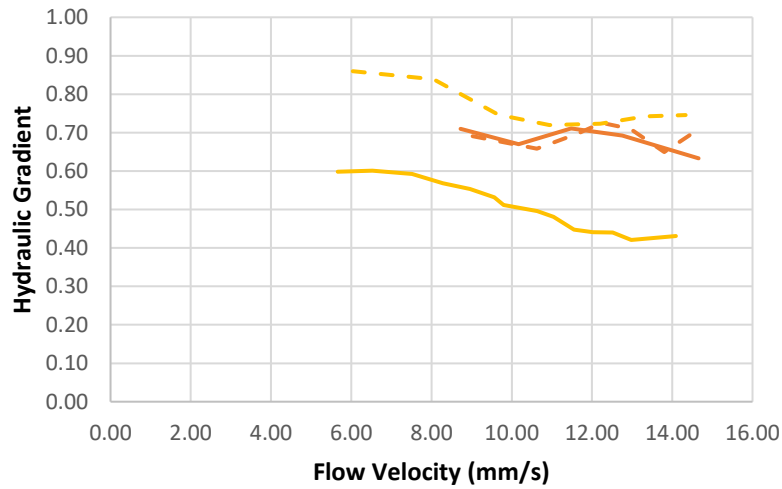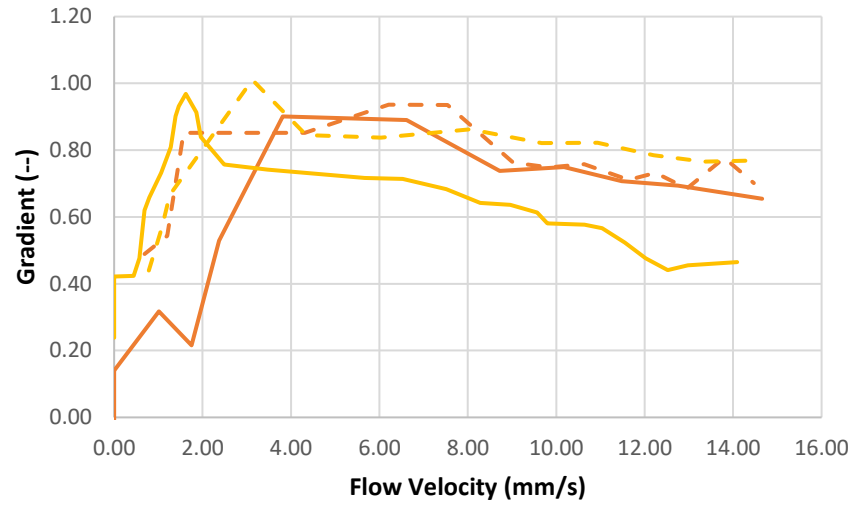
Figure 16: Permeameter Diameter Comparison of Hydraulic Gradients verses Flow Velocities for a) P1-2; b) P1-3; and c) P2-3

Figure 17: Sand Gradation Comparison of Hydraulic Gradients verses Flow Velocities for a) P1-2; b) P1-3; and c) P2-3

Sand Boil Gradients
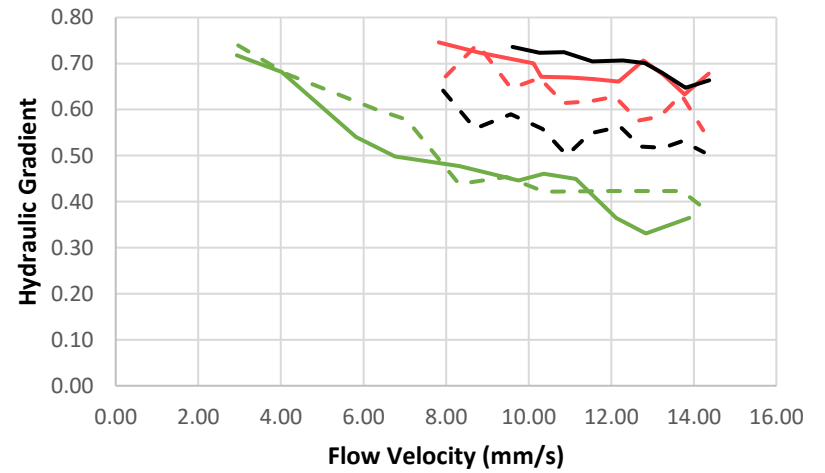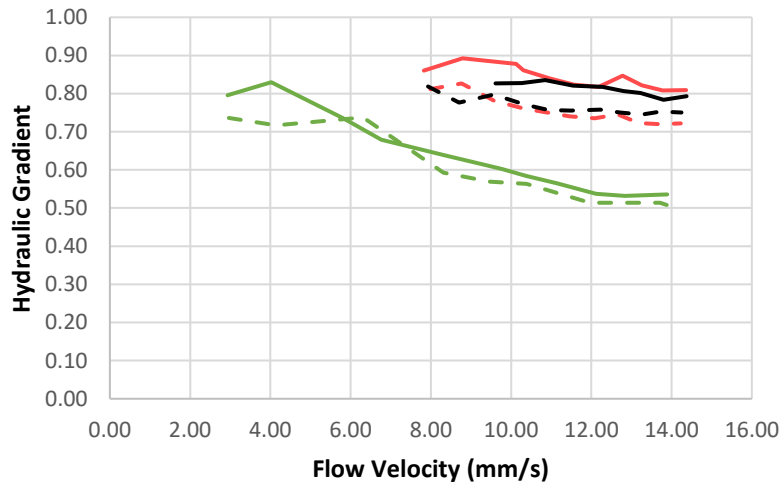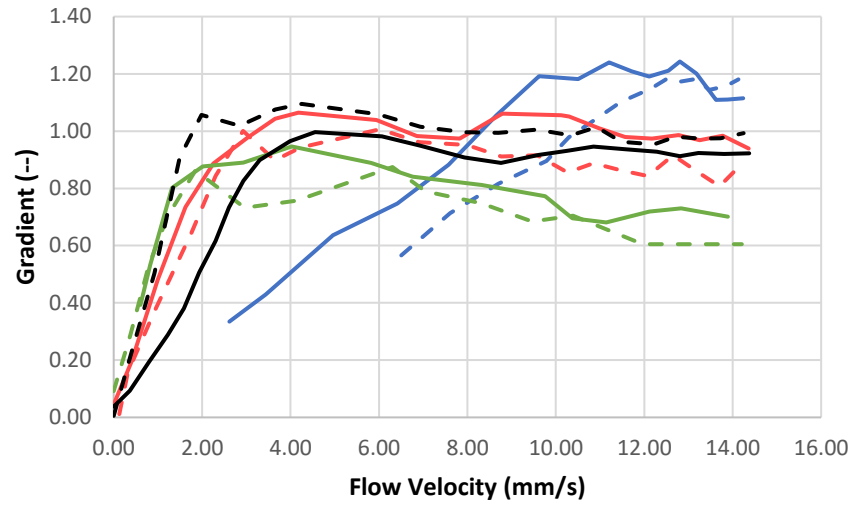
Figure 18 and Table 8 show the average sand boil gradients, maximum gradients, and minimum gradients for the coarse-grained, medium-grained, fine-grained, and well-graded sands. Table 8 also included the theoretical critical (maximum) gradient for each test, which were calculated using Equation 4. The values plotted on Figure 18 are the average value for each sand type and permeameter combination.

The lowest gradients at which sand boils were observed were in the well-graded sand (0.29 and 0.19), while the highest were in the coarse-grained sand (1.24 and 1.18). From these data, it appears that for uniform sand, the sand boil gradient decreases as grain size decreases. This observation does not seem to apply to the well-graded sand. One possible explanation for the low value of the sand boil gradient for the well-graded sand is that suffusion occurred, causing the finer sand particles to wash out of the coarser sand matrix, resulting in boils of fine-grained sand at relatively low gradients, while the coarser structure of the sand remained intact. When the well-graded tests were dismantled, finer grained material was found to be overlying coarser material, supporting this speculation. The highest maximum and minimum gradients occurred in the coarse-grained sand, while the lowest occurred in the fine-grained sand. The well-graded sand and medium-grained sand recorded similar maximum and minimum gradients.

The actual maximum gradients were lower for every test than the theoretical values calculated from Equation 4. The calculation of Equation 4 assumed uniform density throughout the sand column, and this assumption could be inaccurate throughout the course of the tests. Even if sand was initially placed uniformly, the presence of sand boils before the fluidization of the columns indicated that pipes were in the process of forming within the sand columns, which makes the uniformity of the density of the sand questionable. From these tests, it appears that, although the physics of Equation 4 ought to hold true for a given setup, the input parameters may be unknown by the tester, making the estimation of critical gradients more challenging.

It is interesting to note the differences between the sand boil, maximum, and minimum gradients for each specimen. For the coarse-grained sand, all three gradients were closely spaced, indicating little change in the resistance to piping over the course of the tests. For the medium-grained, fine-grained, and well-graded sands, the difference between the sand boil gradient and the maximum gradient was larger, and the difference between the max and min was larger, indicating that resistance to piping decreased as the tests progressed. For the well-graded sand, the difference between the boil and max gradient was the largest, and the difference between the max and min was comparable to the medium-grained sand. This supports the speculation that suffusion occurred initially in the well-graded sand, resulting in boils at low gradients, but also accounting for the sand maintaining resistance to piping due to its coarse- and medium-grained matrix.

It should be reemphasized that the minimum gradients plotted on Figure 18 are not necessarily representative of the lowest possible gradients within each material but represent the lowest gradients that could be obtained for the maximum possible differential hydraulic head within the constraints of the experiment design.
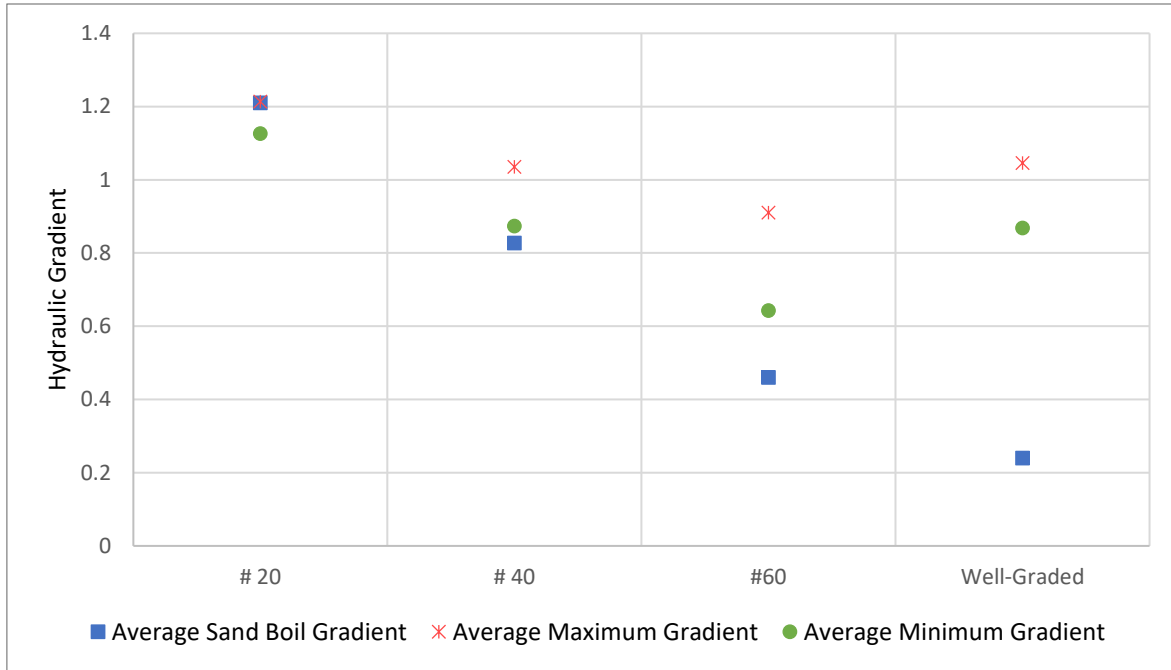
Figure 18: Average Sand Boil, Maximum, and Post-Fluidization Minimum Gradients

Table 8: Sand Boil, Maximum, and Minimum Gradients

		Sand Boil Gradient	Maximum Gradient	Minimum Gradient	Theoretical Maximum (Critical) Gradient[1]
Coarse-Grained	**Test 5**	1.24	1.24	1.11	1.58
	Test 6	1.18	1.18	1.14	1.55
	Avg	1.21	1.21	1.13	1.57
Medium-Grained	**Test 7**	0.98	1.06	0.94	1.49
	Test 8	0.84	1.01	0.81	1.51
	Avg	0.91	1.04	0.87	1.50
Fine-Grained	**Test 9**	0.39	0.95	0.68	1.35
	Test 10	0.53	0.87	0.60	1.37
	Avg	0.46	0.91	0.64	1.36
Well-Graded	**Test 11**	0.29	1.00	0.78	1.48
	Test 12	0.19	1.10	0.95	1.59
	Avg	0.24	1.05	0.87	1.54

[1]Calculated from Equation 4

Summary and Conclusions

This study evaluated the influence of diameter and grain size on the initiation and continuation phase of piping erosion. Twelve tests were performed in a laboratory setting in which sand was fluidized in a controlled setting and hydraulic gradients within the sand, flow rates through the sand, and expansion of the sand columns were measured as the sand was fluidized. This study was conducted to improve the understanding of the resistance a vertical column of sand offers to piping erosion.

From the fluidization tests conducted in two permeameters with different diameters, it cannot be concluded that permeameter diameter has a significant influence on a specimen's resistance to piping erosion. Although one test conducted in the smaller diameter permeameter did record hydraulic gradients lower than those recorded in tests conducted in the larger diameter permeameter, this was not a consistent observation for all tests run in the smaller diameter permeameter. Further analysis ought to involve more tests run in each permeameter as well as incorporating additional permeameters with both larger and smaller diameters than those used in this study.

From the fluidization tests conducted using the well-graded, coarse-, medium-, and fine-grained sands, it appears that resistance to piping is dependent on grain size and grain size distribution. The coarse-grained sand offered the most resistance to piping, the fine-grained sand offered the least, and the medium-grained and well-graded sands offered similar resistances between those of the coarse-grained and fine-grained sands.

Gradients at which sand boils were observed, maximum gradients reached before the sand fluidized, and the minimum gradients reached at the conclusion of each test also appear to be influenced by grain size and grain size distribution. Tests conducted on the coarse-grained sand recorded the highest and most closely spaced sand boil, maximum, and minimum gradients, indicating that it offered the highest and most constant resistance to piping, while the fine-grained sand tests recorded the lowest sand boil, maximum, and minimum gradients, indicating that it offered the least resistance to piping and that resistance decreased as the tests progressed. The medium-grained sand tests recorded sand boil, maximum, and minimum gradients between those of the coarse-grained and fine-grained sands. The well-graded sand tests recorded the lowest sand boil gradient, which could be indicative of the occurrence of suffusion erosion occurring in conjunction with piping erosion, whereby the finer particles were washed out of the sand matrix at relatively low gradients, forming sand boils while the relatively coarser matrix remained resistant to piping. All tests recorded maximum gradients that were lower than the theoretical critical gradients calculated using Equation 4. This is likely due to the changes in the internal configuration of the sand as the piping process

initiates. In order to better understand the influence of gradation on resistance to piping, more sand gradations should be tested in future work.

Measured hydraulic gradients in the lower portion of the fluidized sands were higher than those measured in higher portions. This could be explained if the density of the fluidized sand was not uniform, with more material near the base of the column than near the top, which is contrary to the findings of Sellmeijer. Furthermore, the tests were terminated when the maximum height of the upstream reservoir was reached but did not give any evidence that gradients had leveled off to a uniform "final gradient". It is likely that gradients would have continued to dissipate had more hydraulic head been applied to the upstream reservoir. In order to better understand this, additional testing should be conducted using an upstream reservoir capable of simulating higher hydraulic heads.

Acknowledgements

References

Bezuijen, A. (2015). Critical vertical gradients in piping.

Bligh, W. G. (1910). Dams, Barrages and Weirs on Porous Foundations. *Engineering News, 64*(26), 708-710.

Bligh, W. G. (1915). *Dams and Weirs.* Chicago: American Technical Society.

Bonelli, S. (2013). Introduction. In S. Bonelli, *Fell, R., & Fry, J. (2013). State of the art on the likelihood of internal erosion of dams and levees by means of testing. In Erosion in Geomechanics Applied to Dams and Levees* (pp. xv-xix).

Brown, A., & Bridle, R. (2008). Progress in assessing internal erosion. *15th British Dam Society Biennial Conference.* Coventry, England.

Casagrande, A. (1937). Seepage Through Dams. *Journal of the New England Water Works Association, 51*(2), 295-337.

Fell, R., & Fry, J. (Eds.). (2005). *Internal Erosion of Dams and Their Foundations: Selected Papers from the Workshop on Internal Erosionand Piping of Dams and Their Foundations, Aussois, France, 25-27 April 2005.* Taylor & Grancis Group.

Fell, R., & Fry, J.-J. (2007). The state of the art of assessing the likelihood of internal erosion of embankment dams, water retaining structures and their foundations. In R. Fell, & J.-J. Fry, *Internal Erosion of Dams and Their Foundations: Selected Papers from the Workshop on Internal Erosion and Piping of Dams and Their Foundations, Aussois, France, 25-27 April 2005. Taylor & Grancis Group* (pp. 1-23).

Fell, R., & Fry, J.-J. (2013). State of the art on the likelihood of internal erosion of dams and levees by means of testing. In S. Bonelli, *Erosion in Geomechanics Applied to Dams and Levees* (pp. 1-99).

Forchheimer, P. (1914). *Hydraulik.* Leipzig: B.G. Teubner.

Griffith, W. M. (1913). The Stability of Weir Foundations on Sandy Soil Subject to Hydrostatic Pressure. *Minutes of Proceedings of the Institution of Civil Engineers, 197*(3), 221-232.

Koelewijn, A. R. (2009). *SBW Hervalidatie piping E. Evaluatie 0, 3d rekenregel.* Deltares.

Koenig, A. C. (1911). *Dams on Sand Foundations : Some Principles Involved in Their Designs, and the Law Governing the Depth of Penetration Required for Street-Piling.* ASCE Trans.

Lane, E. W. (1935). Security from under-seepage-masonry dams on earth foundations. *Transactions of the American Society of Civil Engineers, 100*(1), 1235-1272.

Mattsson, H., Hellstrom, G., & Lundstrom, T. (2008). *On internal erosion in embankment dams: a literature survey of the phenomenon and the prospect to model it numerically.*

Rice, J., & Swainston-Fleshman, M. (2013). Laboratory Modeling of Critical Hydraulic Conditions for the Initiation of Piping. *Geo-Congress 2013@ Stability and Performance of Slopes and Embankments III* (pp. 1044-1055). ASCE.

Robbins, B. A. (2014). *Discussions on Laboratory Testing of Backwards Erosion Piping of Soil: An Interview with John H. Schmertmann and Frank C. Townsend.* ENGINEER RESEARCH AND DEVELOPMENT CENTER VICKSBURG MS GEOTECHNICAL AND STRUCTURES LAB: No. ERDC/GSL-TN-14-3.

Sellmeijer, J. B. (1981). Piping due to flow towards ditches and holes. *Proceedings of Euromech 143*, (pp. 69-72). Delft, Netherlands.

Sellmeijer, J. B., & Koenders, M. A. (1991). A Mathematical Model for Piping. *Applied Mathematical Modelling, 15*(11), 646-651.

Skempton, A. W. (1984). Weirs on Permeable Foundations. In *Selected Papers on Soil Mechanics* (p. 264).

Terzaghi, K., & Peck, R. B. (1948). Soil Mechanics in Engineering Practices. New York: John Wiley & Sons, Inc.

Van Beek, V. M. (2015). *Backward erosion piping: initiation and progression.* Delft University of Technology.

Van Beek, V., Bezuijen, A., & Sellmeijer, H. (2013). Backward Erosion Piping. In S. Bonelli, & S. Bonelli (Ed.), *Erosion in Geomechanics Applied to Dams and Levees* (pp. 193-269). John Wiley & Sons.

Yap, H. (1981). *Fluïdisatieproeven op strandzand.* Delft: Laboratorium voor Grondmechanica.

Appendix A – Test Data

Test 1

Time After Start (min)	Differential Head (cm)	Total Sand Height (cm)	Δsand Height (cm)	Density (g/cm3)	Flow Rate (mm/s)	P1-2	P1-3	P1-4	P2-3	P2-4	P3-4
27.04	0.00	24.80	0.00	2.16	0.00	-0.05	--	--	--	--	--
32.04	16.40	24.80	0.00	2.16	0.00	0.14	--	--	--	--	--
60.04	19.30	24.80	0.00	2.16	1.01	0.32	--	--	--	--	--
86.04	25.00	25.00	0.20	2.14	1.75	0.22	--	--	--	--	--
92.04	37.00	25.20	0.40	2.13	2.37	0.53	--	--	--	--	--
123.04	60.10	28.10	3.30	1.91	3.81	0.90	--	--	--	--	--
155.04	100.00	28.20	3.40	1.90	6.61	0.89	--	--	--	--	--
185.04	133.30	30.30	5.50	1.77	8.72	0.74	0.71	--	0.68	--	--
222.04	162.50	31.80	7.00	1.68	10.17	0.75	0.67	--	0.59	--	--
254.04	196.00	31.80	7.00	1.68	11.48	0.71	0.71	--	0.71	--	--
286.04	223.70	32.40	7.60	1.65	12.75	0.69	0.69	--	0.69	--	--
336.04	273.30	33.50	8.70	1.60	14.66	0.65	0.63	--	0.61	--	--

Test 2

Time After Start (min)	Differential Head (cm)	Total Sand Height (cm)	Δsand Height (cm)	Density (g/cm3)	Flow Rate (mm/s)	P1-2	P1-3	P1-4	P2-3	P2-4	P3-4
25.58	15.30	22.70	0.00	2.36	0.69	0.49	--	--	--	--	--
28.58	21.00	21.70	0.00	2.47	1.20	0.54	--	--	--	--	--
89.58	31.50	21.70	0.00	2.47	1.57	0.85	--	--	--	--	--
111.58	62.30	25.00	3.30	2.14	4.31	0.85	--	--	--	--	--
111.58	87.00	27.00	5.30	1.98	6.21	0.94	--	--	--	--	--
129.58	106.30	28.40	6.70	1.89	7.54	0.94	--	--	--	--	--
157.58	133.70	29.40	7.70	1.82	9.03	0.76	0.69	--	0.62	--	--
202.58	149.00	30.40	8.70	1.76	9.84	0.75	0.67	--	0.60	--	--
222.58	168.00	31.00	9.30	1.73	10.63	0.76	0.66	--	0.56	--	--
242.58	195.30	31.50	9.80	1.70	11.64	0.71	0.70	--	0.68	--	--
262.58	211.00	31.70	10.00	1.69	12.25	0.73	0.73	--	0.72	--	--
331.58	229.20	31.80	10.10	1.68	12.96	0.68	0.71	--	0.73	--	--
351.58	254.90	31.90	10.20	1.68	13.80	0.78	0.65	--	0.52	--	--
374.58	273.30	33.50	11.80	1.60	14.47	0.70	0.70	--	0.69	--	--

Test 3

Time After Start (min)	Differential Head (cm)	Total Sand Height (cm)	Δsand Height (cm)	Density (g/cm3)	Flow Rate (mm/s)	P1-2	P1-3	P1-4	P2-3	P2-4	P3-4
30.69	0.00	24.10	0.00	1.35	0.00	0.24	--	--	--	--	--
48.69	2.00	24.10	0.00	1.35	0.00	0.33	--	--	--	--	--
62.69	5.60	24.10	0.00	1.35	0.00	0.42	--	--	--	--	--
65.69	8.90	24.10	0.00	1.35	0.44	0.42	--	--	--	--	--
78.69	12.20	24.10	0.00	1.35	0.57	0.48	--	--	--	--	--
93.69	15.30	24.10	0.00	1.35	0.69	0.62	--	--	--	--	--
97.69	18.20	24.10	0.00	1.35	0.80	0.66	--	--	--	--	--
113.69	23.90	24.10	0.00	1.35	1.06	0.73	--	--	--	--	--
123.69	29.00	24.10	0.00	1.35	1.28	0.81	--	--	--	--	--
133.69	31.50	24.10	0.00	1.35	1.39	0.90	--	--	--	--	--
143.69	33.80	24.10	0.00	1.35	1.46	0.93	--	--	--	--	--
153.69	36.10	24.20	0.10	1.34	1.62	0.97	--	--	--	--	--
163.69	38.40	24.30	0.20	1.34	1.86	0.91	--	--	--	--	--
173.69	42.60	24.40	0.30	1.33	1.96	0.84	--	--	--	--	--
183.69	50.30	24.50	0.40	1.33	2.49	0.76	--	--	--	--	--
193.69	62.30	26.50	2.40	1.23	3.48	0.74	--	--	--	--	--
203.69	87.00	31.30	7.20	1.04	5.66	0.72	0.60	--	0.48	--	--
213.69	99.10	32.40	8.30	1.00	6.52	0.71	0.60	--	0.49	--	--
223.69	113.30	33.40	9.30	0.97	7.51	0.68	0.59	--	0.50	--	--
233.69	127.00	33.60	9.50	0.97	8.28	0.64	0.57	--	0.49	--	--
243.69	138.40	34.40	10.30	0.94	8.96	0.64	0.55	--	0.47	--	--
253.69	149.00	35.40	11.30	0.92	9.57	0.61	0.53	--	0.45	--	--
263.69	161.30	36.00	11.90	0.90	9.80	0.58	0.51	--	0.44	--	--
273.69	173.10	37.30	13.20	0.87	10.64	0.58	0.50	0.51	0.41	0.47	0.53
283.69	185.20	37.80	13.70	0.86	11.04	0.57	0.48	0.50	0.40	0.47	0.55
293.69	199.10	39.00	14.90	0.83	11.55	0.52	0.45	0.49	0.37	0.47	0.56
303.69	211.00	39.80	15.70	0.82	12.02	0.48	0.44	0.48	0.41	0.48	0.55
313.69	223.70	42.00	17.90	0.77	12.52	0.44	0.44	0.47	0.44	0.48	0.52
323.69	235.20	43.00	18.90	0.76	12.98	0.45	0.42	0.45	0.39	0.45	0.51
334.70	273.30	44.00	19.90	0.74	14.09	0.46	0.43	0.46	0.40	0.46	0.52

Test 4

Time After Start (min)	Differential Head (cm)	Total Sand Height (cm)	Δsand Height (cm)	Density (g/cm3)	Flow Rate (mm/s)	P1-2	P1-3	P1-4	P2-3	P2-4	P3-4
8.00	15.5	25.30	0.00	1.28	0.78	0.44	--	--	--	--	--
37.00	18.5	25.30	0.00	1.28	1.08	0.57	--	--	--	--	--
74.00	24.1	25.30	0.00	1.28	1.26	0.67	--	--	--	--	--
99.00	48.3	25.40	0.10	1.28	3.12	1.01	--	--	--	--	--
125.00	62.3	27.30	2.00	1.19	4.34	0.85	--	--	--	--	--
157.00	87	29.00	3.70	1.12	6.04	0.84	0.86	--	0.88	--	--
178.00	117	31.40	6.10	1.04	8.05	0.86	0.84	--	0.81	--	--
198.00	149	34.60	9.30	0.94	9.67	0.82	0.75	--	0.67	--	--
219.00	179.1	36.90	11.60	0.88	10.94	0.82	0.72	--	0.62	--	--
239.00	211	38.20	12.90	0.85	12.20	0.78	0.72	0.61	0.66	0.52	0.37
259.00	240.6	40.50	15.20	0.80	13.33	0.77	0.74	0.61	0.72	0.53	0.35
279.00	273.3	43.70	18.40	0.74	14.33	0.77	0.75	0.60	0.72	0.52	0.32

Test 5

Time After Start (min)	Differential Head (cm)	Total Sand Height (cm)	Δsand Height (cm)	Density (g/cm3)	Flow Rate (mm/s)	P1-2	P1-3	P1-4	P2-3	P2-4	P3-4
84.02	44.6	23.70	0	2.57	2.62	0.33	--	--	--	--	--
103.02	40.7	23.70	0	2.57	3.44	0.43	--	--	--	--	--
121.02	62.3	23.70	0	2.57	4.96	0.636	--	--	--	--	--
143.02	87	23.70	0	2.57	6.42	0.747	--	--	--	--	--
163.02	106.9	23.70	0	2.57	7.57	0.883	--	--	--	--	--
184.02	127.9	23.70	0	2.57	8.65	1.055	--	--	--	--	--
204.02	149	23.70	0	2.57	9.62	1.191	--	--	--	--	--
224.02	169.9	23.70	0	2.57	10.51	1.181	--	--	--	--	--
244.02	188.9	24.10	0.4	2.53	11.20	1.24	--	--	--	--	--
264.02	201.8	24.20	0.5	2.52	11.72	1.208	--	--	--	--	--
304.02	211	24.30	0.6	2.51	12.11	1.191	--	--	--	--	--
324.02	223.1	24.30	0.6	2.51	12.54	1.21	--	--	--	--	--
344.02	231.9	24.40	0.7	2.50	12.81	1.243	--	--	--	--	--
364.02	242	24.50	0.8	2.49	13.18	1.201	--	--	--	--	--
384.02	252.6	24.60	0.9	2.48	13.62	1.109	--	--	--	--	--
404.02	263.2	24.70	1	2.47	13.88	1.11	--	--	--	--	--
428.02	273.3	24.80	1.1	2.46	14.24	1.115	--	--	--	--	--

Test 6

Time After Start (min)	Differential Head (cm)	Total Sand Height (cm)	Δsand Height (cm)	Density (g/cm3)	Flow Rate (mm/s)	P1-2	P1-3	P1-4	P2-3	P2-4	P3-4
38.12	87	24.20	0.00	2.52	6.50	0.57	--	--	--	--	--
58.12	107.8	24.20	0.00	2.52	7.61	0.714	--	--	--	--	--
78.12	127.3	24.20	0.00	2.52	8.70	0.816	--	--	--	--	--
98.12	149	24.20	0.00	2.52	9.79	0.896	--	--	--	--	--
118.12	164	24.20	0.00	2.52	10.30	0.978	--	--	--	--	--
138.12	179.4	24.20	0.00	2.52	10.94	1.045	--	--	--	--	--
158.12	194.2	24.20	0.00	2.52	11.48	1.102	--	--	--	--	--
178.12	211	24.30	0.10	2.51	12.14	1.149	--	--	--	--	--
198.12	221.5	24.30	0.10	2.51	12.52	1.184	--	--	--	--	--
218.12	231.1	24.40	0.20	2.50	12.81	1.173	--	--	--	--	--
238.12	241.3	24.50	0.30	2.49	13.19	1.183	--	--	--	--	--
268.12	251.4	24.60	0.40	2.48	13.47	1.144	--	--	--	--	--
288.12	261.5	24.70	0.50	2.47	13.84	1.157	--	--	--	--	--
318.12	273.3	24.80	0.60	2.46	14.13	1.18	--	--	--	--	--

Test 7

Time After Start (min)	Differential Head (cm)	Total Sand Height (cm)	Δsand Height (cm)	Density (g/cm3)	Flow Rate (mm/s)	P1-2	P1-3	P1-4	P2-3	P2-4	P3-4
37.33	0.00	25.20	0.00	2.42	0.00	0.04	0.03	--	0.01	--	--
57.33	4.80	25.20	0.00	2.42	0.40	0.19	0.15	--	0.10	--	--
77.33	15.30	25.20	0.00	2.42	1.00	0.48	0.40	--	0.33	--	--
97.33	25.00	25.20	0.00	2.42	1.62	0.73	0.59	--	0.44	--	--
117.33	35.00	25.20	0.00	2.42	2.26	0.89	0.74	--	0.60	--	--
137.33	45.80	25.20	0.00	2.42	3.03	0.98	0.85	--	0.72	--	--
157.33	55.20	25.20	0.00	2.42	3.65	1.04	0.88	--	0.71	--	--
177.33	62.30	26.00	0.80	2.34	4.18	1.06	0.88	--	0.70	--	--
197.33	87.00	27.80	2.60	2.19	5.95	1.04	0.90	--	0.76	--	--
217.33	102.00	28.30	3.10	2.15	6.85	0.98	0.87	--	0.76	--	--
237.33	117.00	29.30	4.10	2.08	7.83	0.97	0.86	--	0.75	--	--
257.33	132.00	29.90	4.70	2.04	8.79	1.06	0.89	--	0.72	--	--
282.33	149.00	30.90	5.70	1.97	10.12	1.06	0.88	--	0.70	--	--
302.33	164.00	31.00	5.80	1.96	10.30	1.05	0.86	--	0.67	--	--
322.33	179.00	31.50	6.30	1.93	10.98	1.01	0.84	--	0.67	--	--
342.33	194.00	32.00	6.80	1.90	11.56	0.98	0.82	--	0.67	--	--
362.33	211.00	32.30	7.10	1.89	12.18	0.97	0.82	--	0.66	--	--
382.33	226.00	32.80	7.60	1.86	12.78	0.99	0.85	--	0.71	--	--
402.33	241.00	33.30	8.10	1.83	13.26	0.97	0.82	--	0.68	--	--
422.33	256.00	33.30	8.10	1.83	13.78	0.98	0.81	--	0.63	--	--
453.33	273.30	33.90	8.70	1.80	14.36	0.94	0.81	--	0.68	--	--

Test 8

Time After Start (min)	Differential Head (cm)	Total Sand Height (cm)	Δsand Height (cm)	Density (g/cm3)	Flow Rate (mm/s)	P1-2	P1-3	P1-4	P2-3	P2-4	P3-4
83.99	0.00	24.90	0.00	2.45	0.00	-0.08	-0.04	--	0.00	--	--
103.99	5.30	24.90	0.00	2.45	0.32	0.16	0.07	--	-0.02	--	--
123.99	15.00	24.90	0.00	2.45	0.92	0.37	0.29	--	0.21	--	--
143.99	25.10	24.90	0.00	2.45	1.76	0.64	0.48	--	0.33	--	--
163.99	35.00	24.90	0.00	2.45	2.31	0.84	0.64	--	0.44	--	--
183.99	45.60	25.00	0.10	2.44	2.93	1.00	0.78	--	0.56	--	--
203.99	55.00	25.30	0.40	2.41	3.64	0.90	0.76	--	0.63	--	--
223.99	62.30	25.80	0.90	2.36	4.22	0.94	0.79	--	0.63	--	--
243.99	87.00	27.50	2.60	2.21	6.02	1.01	0.83	--	0.65	--	--
263.99	101.50	28.30	3.40	2.15	6.90	0.96	0.83	--	0.70	--	--
283.99	117.00	29.10	4.20	2.09	7.99	0.95	0.81	--	0.67	--	--
298.99	132.10	29.70	4.80	2.05	8.76	0.91	0.83	--	0.74	--	--
323.99	149.00	30.20	5.30	2.02	9.57	0.92	0.78	--	0.65	--	--
343.99	164.10	30.80	5.90	1.98	10.27	0.86	0.76	--	0.67	--	--
373.99	179.00	31.20	6.30	1.95	10.85	0.89	0.75	--	0.61	--	--
393.99	194.00	31.50	6.60	1.93	11.46	0.86	0.74	--	0.62	--	--
413.99	211.00	32.10	7.20	1.90	12.08	0.84	0.74	--	0.63	--	--
433.99	226.00	32.40	7.50	1.88	12.66	0.92	0.75	--	0.58	--	--
453.99	241.00	33.00	8.10	1.85	13.18	0.86	0.72	--	0.58	--	--
473.99	256.10	33.40	8.50	1.82	13.70	0.81	0.72	--	0.63	--	--
504.99	273.30	33.50	8.60	1.82	14.23	0.89	0.72	--	0.55	--	--

Test 9

Time After Start (min)	Differential Head (cm)	Total Sand Height (cm)	Δsand Height (cm)	Density (g/cm3)	Flow Rate (mm/s)	P1-2	P1-3	P1-4	P2-3	P2-4	P3-4
76.97	14.70	27.80	0.00	2.19	0.61	0.39	--	--		--	--
96.97	20.50	27.80	0.00	2.19	0.83	0.53	--	--		--	--
116.97	28.40	27.80	0.00	2.19	1.32	0.80	--	--		--	--
146.97	41.90	28.00	0.20	2.18	2.01	0.88	--	--		--	--
166.97	51.20	28.90	1.10	2.11	2.93	0.89	0.80	--	0.72	--	--
186.97	62.30	29.50	1.70	2.06	4.02	0.95	0.83	--	0.68	--	--
206.97	87.00	30.90	3.10	1.97	5.82	0.89	0.74	--	0.54	--	--
226.97	102.60	34.80	7.00	1.75	6.77	0.84	0.68	--	0.50	--	--
252.97	127.00	38.10	10.30	1.60	8.32	0.81	0.64	0.58	0.48	0.67	0.52
276.97	149.00	44.60	16.80	1.37	9.76	0.77	0.60	0.56	0.45	0.63	0.50
301.97	170.70	47.50	19.70	1.28	10.37	0.70	0.58	0.52	0.46	0.58	0.42
326.97	189.30	50.00	22.20	1.22	11.14	0.68	0.56	0.51	0.45	0.58	0.42
351.97	211.00	52.50	24.70	1.16	12.12	0.72	0.54	0.50	0.36	0.54	0.45
376.97	230.90	55.10	27.30	1.11	12.84	0.73	0.53	0.47	0.33	0.47	0.38
380.00	273.30	60.60	32.80	1.01	13.89	0.70	0.54	0.49	0.36	0.55	0.45

Test 10

Time After Start (min)	Differential Head (cm)	Total Sand Height (cm)	Δsand Height (cm)	Density (g/cm3)	Flow Rate (mm/s)	P1-2	P1-3	P1-4	P2-3	P2-4	P3-4
58.32	0.00	27.20	-0.20	2.24	0.00	0.09	--	--	--	--	--
78.32	10.20	27.20	-0.20	2.24	0.38	0.29	--	--	--	--	--
98.32	20.20	27.30	-0.10	2.23	0.78	0.53	--	--	--	--	--
148.32	30.30	27.40	0.00	2.22	1.21	0.70	--	--	--	--	--
168.32	40.20	28.40	1.00	2.14	1.85	0.86	--	--	--	--	--
188.32	50.60	29.60	2.20	2.06	2.97	0.73	0.74	--	0.74	--	--
208.32	62.30	30.50	3.10	2.00	4.14	0.76	0.72	--	0.68	--	--
228.32	87.00	33.80	6.40	1.80	6.31	0.87	0.74	--	0.60	--	--
248.32	107.00	38.10	10.70	1.60	7.05	0.79	0.68	0.61	0.58	0.70	0.47
268.32	127.10	41.20	13.80	1.48	8.31	0.75	0.59	0.57	0.44	0.64	0.53
288.32	149.00	45.30	17.90	1.34	9.46	0.68	0.57	0.55	0.45	0.64	0.50
308.32	164.58	46.80	19.40	1.30	10.38	0.70	0.56	0.56	0.42	0.64	0.54
328.32	189.20	49.80	22.40	1.22	11.97	0.61	0.51	0.52	0.42	0.64	0.53
328.32	211.00	52.60	25.20	1.16	12.13	0.61	0.51	0.52	0.42	0.64	0.53
328.32	226.40	54.30	26.90	1.12	12.65	0.61	0.51	0.52	0.42	0.64	0.53
328.32	241.00	56.00	28.60	1.09	13.18	0.61	0.51	0.52	0.42	0.64	0.53
328.32	256.00	57.00	29.60	1.07	13.71	0.61	0.51	0.52	0.42	0.64	0.53
431.32	273.30	59.00	31.60	1.03	14.21	0.60	0.50	0.46	0.39	0.51	0.38

Test 11

Time After Start (min)	Differential Head (cm)	Total Sand Height (cm)	Δsand Height (cm)	Density (g/cm3)	Flow Rate (mm/s)	P1-2	P1-3	P1-4	P2-3	P2-4	P3-4
38.44	0.00	25.30	0.00	2.41	0.00	0.04	--	--	--	--	--
58.44	4.90	25.30	0.00	2.41	0.36	0.09	--	--	--	--	--
78.44	10.00	25.30	0.00	2.41	0.79	0.19	--	--	--	--	--
98.44	15.00	25.30	0.00	2.41	1.23	0.29	--	--	--	--	--
118.44	20.00	25.30	0.00	2.41	1.59	0.38	--	--	--	--	--
138.44	25.00	25.30	0.00	2.41	1.94	0.51	--	--	--	--	--
158.44	30.00	25.50	0.20	2.39	2.31	0.62	--	--	--	--	--
178.44	35.00	25.60	0.30	2.38	2.61	0.73	--	--	--	--	--
198.44	40.00	25.80	0.50	2.36	2.94	0.83	--	--	--	--	--
218.44	45.00	25.90	0.60	2.35	3.30	0.90	--	--	--	--	--
238.44	50.00	25.80	0.50	2.36	3.99	0.97	--	--	--	--	--
253.44	55.00	26.00	0.70	2.34	4.56	1.00	--	--	--	--	--
278.44	62.30	26.50	1.20	2.30	6.06	0.98	--	--	--	--	--
298.44	87.00	27.40	2.10	2.22	6.93	0.95	--	--	--	--	--
318.44	102.00	28.00	2.70	2.18	7.94	0.91	--	--	--	--	--
338.44	117.00	28.50	3.20	2.14	8.76	0.89	--	--	--	--	--
358.44	132.00	29.30	4.00	2.08	9.61	0.92	0.83	--	0.74	--	--
378.44	149.00	29.80	4.50	2.04	10.27	0.93	0.83	--	0.72	--	--
398.44	164.00	30.20	4.90	2.02	10.85	0.95	0.84	--	0.72	--	--
418.44	179.00	30.30	5.00	2.01	11.55	0.94	0.82	--	0.70	--	--
438.44	194.00	32.10	6.80	1.90	12.28	0.93	0.82	--	0.71	--	--
458.44	211.00	32.40	7.10	1.88	12.81	0.91	0.81	--	0.70	--	--
478.44	226.00	32.70	7.40	1.86	13.23	0.92	0.80	--	0.68	--	--
498.44	241.00	33.80	8.50	1.80	13.80	0.92	0.78	--	0.65	--	--
499.44	256.00	34.10	8.80	1.79	14.37	0.92	0.79	--	0.66	--	--

Test 12

Time After Start (min)	Differential Head (cm)	Total Sand Height (cm)	Δsand Height (cm)	Density (g/cm3)	Flow Rate (mm/s)	P1-2	P1-3	P1-4	P2-3	P2-4	P3-4
41.79	0.00	23.50	0.00	2.59	0.00	0.01		--		--	--
61.79	5.00	23.50	0.00	2.59	0.34	0.19		--		--	--
81.79	15.00	23.50	0.00	2.59	0.92	0.50		--		--	--
101.79	25.00	23.60	0.10	2.58	1.49	0.91		--		--	--
121.79	35.00	23.60	0.10	2.58	1.98	1.06		--		--	--
171.79	45.00	24.70	1.20	2.47	2.85	1.02		--		--	--
191.79	55.00	25.30	1.80	2.41	3.66	1.08		--		--	--
211.79	62.30	25.40	1.90	2.40	4.25	1.10		--		--	--
231.79	87.00	25.50	2.00	2.39	5.98	1.06		--		--	--
251.79	102.00	26.00	2.50	2.34	6.93	1.02		--		--	--
271.79	117.00	26.50	3.00	2.30	7.93	1.00	0.82	--	0.64	--	--
286.79	132.00	26.80	3.30	2.27	8.70	0.99	0.78	--	0.56	--	--
311.79	149.00	27.50	4.00	2.21	9.57	1.00	0.80	--	0.59	--	--
331.79	164.00	30.50	7.00	2.00	10.34	0.99	0.77	--	0.56	--	--
351.79	179.00	31.20	7.70	1.95	10.92	1.01	0.76	--	0.50	--	--
371.79	194.00	32.20	8.70	1.89	11.48	0.96	0.76	--	0.55	--	--
391.79	211.00	32.60	9.10	1.87	12.22	0.95	0.76	--	0.56	--	--
411.79	226.00	33.40	9.90	1.82	12.71	0.98	0.75	--	0.52	--	--
431.79	241.00	34.60	11.10	1.76	13.26	0.97	0.74	--	0.52	--	--
451.79	256.00	34.70	11.20	1.76	13.73	0.97	0.75	--	0.53	--	--
472.79	273.30	35.50	12.00	1.72	14.25	0.99	0.75	--	0.51	--	--